



UNIVERSITY OF LEEDS

This is a repository copy of *The Ca²⁺ sensor STIM1 regulates type I interferon response by retaining the signaling adaptor STING at the endoplasmic reticulum.*

White Rose Research Online URL for this paper:
<http://eprints.whiterose.ac.uk/140349/>

Version: Accepted Version

Article:

Srikanth, S, Woo, JS, Wu, B et al. (14 more authors) (2019) The Ca²⁺ sensor STIM1 regulates type I interferon response by retaining the signaling adaptor STING at the endoplasmic reticulum. *Nature Immunology*. pp. 152-162. ISSN 1529-2908

<https://doi.org/10.1038/s41590-018-0287-8>

© The Author(s), under exclusive licence to Springer Nature Limited 2019. This is a post-peer-review, pre-copyedit version of an article published in *Nature Immunology*. The final authenticated version is available online at:
<https://doi.org/10.1038/s41590-018-0287-8>.

Reuse

Items deposited in White Rose Research Online are protected by copyright, with all rights reserved unless indicated otherwise. They may be downloaded and/or printed for private study, or other acts as permitted by national copyright laws. The publisher or other rights holders may allow further reproduction and re-use of the full text version. This is indicated by the licence information on the White Rose Research Online record for the item.

Takedown

If you consider content in White Rose Research Online to be in breach of UK law, please notify us by emailing eprints@whiterose.ac.uk including the URL of the record and the reason for the withdrawal request.



eprints@whiterose.ac.uk
<https://eprints.whiterose.ac.uk/>

1 **The Ca²⁺ sensor STIM1 regulates type I interferon response by retaining**
2 **the signaling adaptor STING at the endoplasmic reticulum**

3 **Sonal Srikanth^{1, 14, 15, *}, Jin Seok Woo^{1, 14}, Beibei Wu¹, Yasser M. El-Sherbiny^{2, 3, 4}, Jennifer**
4 **Leung¹, Koollawat Chupradit^{5, 6, 7}, Laura Rice⁸, Gil Ju Seo⁹, Guillaume Calmettes¹⁰, Chandran**
5 **Ramakrishna¹¹, Edouard Cantin¹¹, Dong Sung An^{5, 6, 7}, Ren Sun¹², Ting-Ting Wu¹², Jae U. Jung⁹,**
6 **Sinisa Savic^{2, 13}, and Yousang Gwack^{1, 15 *}**

7 ¹ Department of Physiology, David Geffen School of Medicine, UCLA, Los Angeles, CA 90095, USA

8 ² National Institute for Health Research—Leeds Biomedical Research Centre and Leeds Institute of Rheumatic
9 and Musculoskeletal Medicine (LIRMM), Wellcome Trust Brenner Building, St James's University Hospital,
10 Beckett Street, Leeds, UK

11 ³ Clinical Pathology Department, Faculty of Medicine, Mansoura University, Egypt.

12 ⁴ School of Science and Technology, Department of Biosciences, Nottingham Trent University, Nottingham, UK

13 ⁵ Division of Hematology-Oncology, David Geffen School of Medicine at UCLA, Los Angeles, CA 90095, USA

14 ⁶ School of Nursing, University of California at Los Angeles, Los Angeles, CA 90095, USA

15 ⁷ UCLA AIDS Institute, Los Angeles, CA 90095, USA

16 ⁸ Leeds Institute of Biomedical and Clinical Sciences, University of Leeds, Wellcome Trust Brenner Building, St
17 James's University Hospital, Beckett Street, Leeds, UK

18 ⁹ Department of Molecular Microbiology and Immunology, Keck School of Medicine, University of Southern
19 California, Los Angeles, CA 90033, USA

20 ¹⁰ Department of Medicine (Cardiology), David Geffen School of Medicine at UCLA, Los Angeles, CA 90095,
21 USA

22 ¹¹ Department of Molecular Immunology, City of Hope Beckman Research Institute, Duarte, CA 91010, USA

23 ¹² Department of Molecular and Medical Pharmacology, UCLA, Los Angeles, CA 90095, USA

24 ¹³ Department of Clinical Immunology and Allergy, St James's University Hospital, Leeds, UK

25 ¹⁴ Equal contribution

26 ¹⁵ Senior author

27 * Corresponding author

28
29 Address correspondence to: Dr. Sonal Srikanth or Dr. Yousang Gwack

30 Department of Physiology

31 David Geffen School of Medicine at UCLA

32 53-266 CHS, 10833 Le Conte Avenue

33 Los Angeles, CA 90095

34 Tel: 310-794-2003; FAX: 310-206-5661

35 email: ssrikanth@mednet.ucla.edu; ygwack@mednet.ucla.edu

36

37 **STING is an endoplasmic reticulum (ER) signaling adaptor that is essential for the type I**
38 **Interferon response to DNA pathogens. Aberrant activation of STING is linked to the pathology**
39 **of autoimmune and autoinflammatory diseases. The rate-limiting step for the activation of**
40 **STING is its translocation from the ER to the ER–Golgi intermediate compartment. Here we**
41 **found that deficiency in the Ca²⁺ sensor STIM1 caused spontaneous activation of STING and**
42 **enhanced expression of type I interferons under resting conditions in mice and a patient**
43 **suffering from combined immunodeficiency. Mechanistically, STIM1 associated with STING to**
44 **retain it in the ER membrane, and co-expression of full-length or a STING-interacting fragment**
45 **of STIM1 suppressed the function of dominant STING mutants that cause autoinflammatory**
46 **diseases. Furthermore, deficiency in STIM1 strongly enhanced the expression of type I**
47 **interferons after viral infection and prevented the lethality of infection with a DNA virus in vivo.**
48 **This work delineates a STIM1–STING circuit that maintains the resting state of the STING**
49 **pathway.**

50

51 The endoplasmic reticulum (ER) provides a structural platform for activation of the type I interferon
52 (IFN) response. Stimulator of interferon genes (STING), a key signaling adaptor protein for DNA-
53 sensing pathways localizes to the ER membrane in the resting state^{1, 2, 3}. After activation by cytosolic
54 DNAs, it translocates into the ER-Golgi intermediate compartment (ERGIC) to recruit TANK-binding
55 kinase 1 (TBK1) and interferon regulatory factor 3 (IRF3). IRF3, upon phosphorylation by TBK1,
56 homo-dimerizes and translocates into the nucleus to induce transcription of type I IFNs^{4, 5, 6, 7}. Beside
57 an essential role in protecting the host against DNA pathogens, STING is also involved in the
58 pathogenesis of autoinflammation caused by self-DNAs in murine models^{8, 9}. Accordingly, STING has
59 been implicated in the pathogenesis of Aicardi–Goutieres syndrome (AGS), systemic lupus
60 erythematosus (SLE) and other type I Interferonopathies¹⁰. Furthermore, mutations in STING have
61 been uncovered in patients with STING-associated vasculopathy with onset in infancy (SAVI) and
62 lupus-like symptoms^{11, 12, 13}. The STING variants found in SAVI patients are constitutively active and

63 localize to the ERGIC without the STING ligand, cyclic dinucleotides (CDNs), suggesting that they
64 may escape a mechanism that potentially maintains the ER localization of STING¹⁴. Since CDNs can
65 be generated by cytosolic self-DNAs derived from mitochondrial damage or genomic instability, and
66 the binding affinity of STING for CDNs is high (~5 nM for 2',3' cyclic guanosine monophosphate-
67 adenosine monophosphate [2',3'-cGAMP])¹⁵, active inhibitory mechanisms are necessary to tightly
68 control its activation. However, little is known about how the resting state of STING is maintained.

69 High Ca^{2+} concentration in the ER ($[\text{Ca}^{2+}]_{\text{ER}}$) is essential for its normal function. At the same
70 time, diverse receptors elevate cytoplasmic $[\text{Ca}^{2+}]$ by depleting ER Ca^{2+} stores through a mechanism
71 called store-operated Ca^{2+} entry (SOCE). Stromal interaction molecule 1 (STIM1), an EF-hand-
72 containing Ca^{2+} -binding protein localizes throughout the ER when $[\text{Ca}^{2+}]_{\text{ER}}$ is high, but after depletion
73 of the ER Ca^{2+} stores, it translocates into junctional areas between the ER and plasma membrane,
74 interacts with the pore subunit of store-operated Ca^{2+} (SOC) channels; Orai1, and induces Ca^{2+}
75 entry¹⁶. The essential role of STIM1 in effector function of adaptive immune cells including T and B
76 cells has been well established^{17, 18, 19}. Mutations in *STIM1* cause severe combined immune deficiency
77 (SCID) in humans²⁰. Paradoxically, these patients also suffer from lymphoproliferative and
78 autoimmune complications. Although for some forms of SCID, the mechanisms behind these
79 complications have been worked out; for example, poor development of both central and peripheral
80 tolerance²¹, the underlying causes of inflammatory complications in patients harboring mutations in
81 *STIM1* are not unknown.

82 The role of STIM1 in cells of the innate immune system is currently unclear. Here, we
83 examined the phenotypes of STIM1-deficient cells and observed that loss of STIM1 induces
84 spontaneous activation of the STING-TBK1-IRF3 pathway to activate type I IFN responses under
85 sterile conditions in both murine and human cells. Mechanistically, STIM1 directly interacted with
86 STING to retain it in an inactive state on the ER membrane. Accordingly, we also observed strong
87 resistance to viral infections in STIM1 KO cells and animals. These results suggest that STIM1 plays

88 an important role in regulation of the innate immune responses in addition to its well-established
89 function in regulation of SOCE in adaptive immunity.

90 **Results**

91 **STIM1 deficiency induces type I IFN response**

92 To gain insights into possible role of STIM1 in innate immune responses, we checked expression of
93 various inflammatory cytokines in *Stim1*^{-/-} murine embryonic fibroblasts (MEFs). Among these,
94 transcripts of *Ifnb1* and *Il6* as well as interferon-stimulated genes (ISGs) were significantly increased
95 in *Stim1*^{-/-} MEFs compared to those in wild type (WT) cells (Fig. 1a). Accordingly, we observed
96 increased amounts of secreted IFN-β protein in culture supernatants from *Stim1*^{-/-} MEFs (Fig. 1b).
97 Due to the well-established role of STIM1 in SOCE, it was possible that the increased type I IFN
98 response in *Stim1*^{-/-} MEFs was due to altered intracellular Ca²⁺ homeostasis. To check this possibility,
99 we compared responses between *Stim1*^{-/-} and *Orai1*^{-/-} MEFs, both of which show loss of SOCE (Fig.
100 1c). However, we did not observe enhanced *Ifnb1* expression in *Orai1*^{-/-} MEFs, indicating that block of
101 SOCE or altered intracellular Ca²⁺ levels do not contribute to increased type I IFN response observed
102 in *Stim1*^{-/-} MEFs.

103 To verify these observations in primary cells, we examined bone marrow-derived
104 macrophages (BMDMs) from WT (*Stim1*^{fl/fl}) and *Stim1*^{fl/fl}UBC-ERT2-cre mice to induce acute loss of
105 STIM1 expression after tamoxifen treatment (Fig. 1d). Similar to MEFs, we observed enhanced
106 expression of *Ifnb1* and *Il6* transcripts in *Stim1*^{-/-} BMDMs. Next, we examined if this enhanced type I
107 IFN expression phenotype was conserved in human macrophages. We generated *STIM1*^{-/-} THP1
108 cells by CRISPR/Cas9-mediated genome editing using two different gRNA sequences
109 (Supplementary Fig. 1). Similar to murine cells, we observed an induction of *IFNB1* and *IL6* mRNAs
110 and increased IFN-β secretion in *STIM1*^{-/-} THP1 clones (Fig. 1e, f). Moreover, exogenous expression
111 of STIM1 in these THP1 clones significantly rescued the phenotype by decreasing type I IFN
112 expression. Taken together, these data strongly demonstrate an inhibitory role of STIM1 in type I IFN

113 responses. STIM2 is another member of the STIM family that shares 66% amino acid sequence
114 similarity with STIM1¹⁶. Both of them are ER-resident proteins, but they function differently in sensing
115 depletion of the ER Ca²⁺ stores and efficacy to activate Orai channels. STIM1 plays a dominant role in
116 activation of SOCE while STIM2 is involved in ER Ca²⁺ homeostasis by sensing subtle changes in
117 [Ca²⁺]_{ER}^{22 23}. To check a possible function of STIM2 in regulation of type I IFN responses, we
118 generated two independent *STIM2*^{-/-} THP1 clones. However, neither of the STIM2 KO clones showed
119 elevated expression of *IFNB1* transcripts (Supplementary Fig. 2). Collectively, these results establish
120 a specific role for STIM1 in regulating the resting state of the type I IFN responses in murine and
121 human cells.

122

123 **STING-TBK1-IRF3 pathway links perturbation in STIM1 expression to IFN-β expression**

124 Since both STIM1 and STING, an important regulator for the type I IFN responses, localize to the ER
125 membrane, we checked the possibility that STIM1 regulates the function of STING. Upon activation of
126 STING via exposure to its ligand 2',3'-cGAMP, we observed a pronounced enhancement of *Irfb1*
127 transcript and protein levels in *Stim1*^{-/-}, but not *Orai1*^{-/-} MEFs when compared to those in WT MEFs
128 (Fig. 2a). This higher type I IFN response in *Stim1*^{-/-} MEFs was also observed in the presence of
129 cytosolic DNAs after transfection with IFN stimulatory DNA (ISD) or poly(dA:dT) that are known to
130 activate the STING pathway, but not with poly(I:C), a poor agonist of the STING pathway (Fig. 2b,
131 left). Similarly, we observed elevated transcripts of *IFNB1* in *STIM1*^{-/-} THP1 cells transfected with
132 2',3'-cGAMP, but not poly(I:C) (Fig. 2b, right).

133 To determine whether deficiency of STIM1 induces an increase in type I IFN response through
134 the STING-TBK1-IRF3 pathway, we checked for activated IRF3 and TBK1 in WT and *Stim1*^{-/-} MEFs.
135 We examined localization of GFP-IRF3, which was exclusively in the cytoplasm in WT MEFs but
136 showed almost equal distribution in the cytoplasm and nuclei in *Stim1*^{-/-} MEFs (Fig. 2c).
137 Biochemically, we detected enhanced homo-dimers of IRF3, in *Stim1*^{-/-} MEFs compared to WT cells
138 under resting conditions (Fig. 2d). Furthermore, we found enhanced levels of phosphorylated TBK1

139 and accordingly increased ratio of p-TBK1 vs. total TBK1 in *Stim1*^{-/-} MEFs, BMDMs and *STIM1*^{-/-}
140 THP1 cells (Fig. 2e). We could also detect enhanced dimerization of endogenous STING in *Stim1*^{-/-}
141 MEFs, which is considered an active form of STING (Supplementary Fig. 3a). Likewise, *STIM1*^{-/-}
142 HEK293T cells stably expressing STING also showed enhanced STING dimers and multimers
143 (Supplementary Fig. 3b). Next, we examined whether co-deletion of STING in STIM1-deficient cells
144 could rescue this enhanced IFN-β expression phenotype. Deletion of both *Stim1* and *Tmem173* (gene
145 encoding STING) in MEFs (double knockout, DKO) dramatically reduced *Irfnb1* and *Il6* transcripts
146 under resting or cGAMP-treated conditions (Fig. 2f). Co-deletion of *Tmem173* also rescued increased
147 IFN-β secretion observed in *Stim1*^{-/-} MEFs treated with poly (dA:dT) (Fig. 2g). We observed very
148 similar results using THP1 cells. Deletion of both *STIM1* and *TMEM173* in double knockout (DKO)
149 THP1 cells was confirmed by immunoblotting and SOCE measurements (Fig. 2h). DKO THP1 cells
150 showed reduced *IFNB1* and *IL6* mRNA levels, suggesting that the elevated cytokine expression in
151 *STIM1*^{-/-} THP1 cells were derived from increased STING activity. Together, these results suggest that
152 the increase in type I IFN responses observed in STIM1-deficient cells is mediated by the STING-
153 TBK1-IRF3 pathway, and STIM1 plays a novel role in type I IFN signaling via regulating STING
154 function.

156 **Increased type I IFN responses in patient lacking STIM1 expression**

157 Previously, patients showing SCID symptoms and bearing homozygous nonsense mutation of STIM1
158 (E136X) were shown to lack STIM1 expression due to nonsense-mediated mRNA decay²⁴. To mimic
159 the phenotype of this patient, we transduced STIM1-deficient cells with viral vectors encoding WT and
160 *STIM1*^{E136X} proteins. We confirmed lack of STIM1 expression in *Stim1*^{-/-} MEFs transduced to express
161 *STIM1*^{E136X} while those with *STIM1*^{WT} showed expression similar to the endogenous protein in WT
162 MEFs (Fig. 3a). Importantly, expression of *STIM1*^{WT} but not *STIM1*^{E136X} rescued the increased type I
163 IFN response in *Stim1*^{-/-} MEFs (Fig. 3b).

164 To examine if this was true in STIM1-deficient patients, we harvested primary cells from a
165 patient lacking STIM1 expression due to a homozygous *STIM1* mutation c.478del, p.(Ser160fs). The
166 lack of STIM1 expression in patient's PBMCs was confirmed by immunoblotting (Fig. 3c). Patient
167 serum showed enhanced IFN- β , IL-6 and TNF cytokines when compared to those observed in three
168 healthy controls (Fig. 3d). Consistently, we also observed enhanced expression of ISGs in PBMCs
169 and monocytes from the patient, when compared to those in two healthy controls (Fig. 3e).
170 Interestingly, the patient also exhibited very mild SAVI-like symptoms – he suffered from
171 desquamation and blistering with skin eruptions mainly affecting the palm, soles of the feet and
172 cheeks. He also showed pronounced nail dystrophy²⁵. Together, these data confirm that loss of
173 STIM1 in humans enhances expression of type I IFN, proinflammatory cytokines and ISGs, similar to
174 murine cells.

175

176 **STIM1 interacts with STING for its retention at the endoplasmic reticulum**

177 The increased type I IFN response together with higher basal activity of the STING-TBK1-IRF3
178 pathway in STIM1-deficient cells suggests that STIM1 may be involved in maintaining the resting state
179 of the STING pathway. Microscopy analysis showed a strong co-localization between STIM1 and
180 STING in the ER (Fig. 4a). Hence, we checked if STIM1 can physically interact with STING to retain it
181 in the ER. When co-expressed in HEK293T cells, STIM1 was specifically identified from
182 immunoprecipitates of STING (Fig. 4b). In addition, we also validated association between
183 endogenous STIM1 and STING proteins by immunoprecipitation (Fig. 4c). This association was
184 specific because another ER-resident protein, calnexin could not be detected in immunoprecipitates of
185 STIM1.

186 Next, we examined association between STIM1 and STING upon activation of either of the
187 proteins. We activated STIM1 by treatment with thapsigargin that depletes the ER Ca²⁺ stores, and
188 activated STING using its ligand, 2',3'-cGAMP. We observed reduced biochemical association
189 between the two proteins by stimulation of either STIM1 or STING (Fig. 4d). These data indicate that

190 STING and STIM1 form a protein complex that is dissociated due to conformational changes induced
191 by stimulation of either of these proteins. Association between STING and STIM1 prompted us to
192 check for a possible role of STING in regulating the function of STIM1. We observed reduced SOCE
193 induced by thapsigargin or anti-CD3 antibody treatment in HEK293T and Jurkat T cells
194 overexpressing STING (Supplementary Fig. 4a, b, c). In addition, we observed enhanced STIM1
195 translocation to the ER-PM junctions in thapsigargin treated STING-deficient (*Tmem173*^{-/-}) MEFs
196 (Supplementary Fig. 4d). Conversely, there was significant enhancement of SOCE in *TMEM173*^{-/-}
197 Jurkat cells (Supplementary Fig. 4e, f). This enhancement was not observed in THP1 cells, indicating
198 cell type specificity (Fig. 2h). Taken together, these data show that association with STING impacts
199 the function of STIM1 in mediating SOCE.

200 STING contains four transmembrane (TM) segments in its N terminus that span the ER
201 membrane (Fig. 4e)¹. STING N-terminal domain (NTD) containing the TM segments plays an
202 important role in its ER localization, trafficking and interaction with regulators including ZDHHC1,
203 AMFR, TRIM32, and RNF5^{26, 27, 28, 29}. Tumor DNA viral proteins, E1A and E7 also bind to STING NTD
204 to inhibit downstream signaling²⁸. The cytoplasmic region (C-terminal domain, CTD) of STING
205 contains the dimerization domain (DD), CDN-binding region, and the C-terminal tail (CTT) that
206 interacts with TBK1 and IRF3. STIM1 has an N-terminal ER-luminal region containing the Ca²⁺-
207 sensing EF-hand motifs and sterile alpha motif (SAM) domain that is important for its multimerization
208 after ER Ca²⁺ depletion. It also has a single TM domain that traverses the ER membrane. The
209 cytoplasmic C terminus contains multiple functional domains including coiled-coil domains (CC) 1,
210 CC2, CC3, a serine/threonine-rich domain (S/T), and a lysine-rich domain (poly-K) that are important
211 for binding to the plasma membrane after depletion of ER Ca²⁺ stores. A fragment containing CC2
212 and CC3 of STIM1 called the CRAC activation domain (CAD) or the STIM1 Orai activating region
213 (SOAR) was identified to interact directly with Orai1 subunits to gate them^{16, 29}.

214 To determine their interaction domains, we carried out co-immunoprecipitation using lysates of
215 HEK293T cells overexpressing full-length, NTD or CTD of STING together with full-length STIM1.

216 These results showed NTD of STING as a major STIM1-interacting domain while its CTD interacted
217 weakly with STIM1 (Fig. 4f, left panels). To uncover the domain(s) of STIM1 involved in interaction
218 with STING, we performed GST pull-down experiments by incubating bacterially purified GST-fused
219 fragments of STIM1 with lysates of HEK293T cells overexpressing full-length, NTD or CTD of STING.
220 From this analysis, we identified a predominant interaction between the N terminus of STIM1
221 containing the TM segment (a.a. 1-249) and STING NTD, and a weaker binding of the cytoplasmic
222 fragment predominantly containing the S/T-rich region of STIM1 to STING CTD (Fig. 4f, right panels).
223 These data suggest that interaction between STIM1 and STING is predominantly mediated by their
224 TM domains on the ER membrane with weak additional interactions between their cytoplasmic
225 regions.

226

227 **STIM1 acts as an ER retention factor to suppress the activity of STING**

228 Ligand binding induces conformational rearrangement and trafficking of STING from the ER to the
229 ERGIC and the Golgi apparatus^{14, 30, 31}. Since STIM1 interacted strongly with STING NTD, which is
230 crucial for STING localization, we hypothesized that STIM1 may control the ER localization of STING.
231 To validate this hypothesis, we examined the localization of STING in WT and *Stim1*^{-/-} MEFs by co-
232 staining with ERGIC marker (ERGIC-53/p58). We observed a significant population of *Stim1*^{-/-} MEFs
233 showing partial localization of STING at the ERGIC without any stimulation, and this population
234 increased much faster in *Stim1*^{-/-} MEFs infected with the DNA virus, herpes simplex virus type-1
235 (HSV-1) when compared to WT MEFs (Fig. 5a). To check how interaction with STIM1 influences the
236 function of STING, we monitored the translocation kinetics of STING after treatment of WT or *Stim1*^{-/-}
237 MEFs with 2',3'-cGAMP and observed faster translocation of STING into the ERGIC in *Stim1*^{-/-} MEFs
238 than in WT cells (Fig. 5b). Together with our biochemical analysis, these data suggest that STIM1
239 physically interacts with STING to promote its retention onto the ER membrane.

240 We checked if overexpression of STIM1 can inhibit the function of STING using *Irfnb* promoter-
241 driven luciferase reporter (IFN-Luc) assays after 2',3'-cGAMP treatment. In cells co-expressing STING

242 and increasing amounts of full length or the N- and C-terminal binding fragments of STIM1, we
243 observed a dose-dependent inhibition of luciferase reporter expression (Fig. 5c). In support of our
244 biochemical analyses, the N-terminal TM-containing fragment of STIM1 (a.a. 1-249) showed a
245 stronger inhibition of luciferase reporter activity than the cytoplasmic domain (a.a. 400-600) while
246 STIM1 fragments (a.a. 250-400 and a.a. 600-685) that do not interact with STING did not affect
247 luciferase activity. Of note, expression of full-length STIM1 or its N-terminal fragment (a.a. 1-249) did
248 not influence the luciferase activity when stimulated with poly(I:C). These data validate functional
249 interaction between STIM1 and STING proteins.

250 The genetic lesions of patients exhibiting autoinflammatory vasculopathy and autoimmunity
251 were mapped to single amino acid substitutions in STING¹¹. These substitution mutations changed
252 one of the conserved residues V147, N154, or V155, all of which are localized in or around the STING
253 dimerization domain³². In addition, these substitutions lead to localization of STING at the ERGIC and
254 constitutive TBK1 and IRF3 activation and uncontrolled type I IFN response^{11, 13}. We examined if
255 these disease-associated STING mutants retained binding to STIM1. Using immunoprecipitation
256 analysis, we observed reduced interaction of the STING SAVI mutants with STIM1 and
257 overexpression of full-length or N-terminal fragment of STIM1 could suppress *Irf3* promoter-driven
258 luciferase activity of these mutants. (Supplementary Fig. 5a, b). In support of these data, confocal
259 analyses showed a partial block of constitutive ERGIC localization of these mutants in the presence of
260 STIM1 (Supplementary Fig. 5c). Collectively, these results confirm the previous observations that exit
261 from the ER is an important step for the activation of STING and STIM1 can block this trafficking via
262 direct interaction.

263

264 **Genetic inhibition of STIM1 expression primes antiviral activity**

265 We sought to determine whether deficiency of STIM1 influences activation of the type I IFNs in
266 response to DNA virus infection. To examine this, WT and *Stim1*^{-/-} MEFs were infected with DNA
267 viruses (e.g., HSV-1 and murine γ -herpesvirus, MHV-68). Spontaneous induction of IFN- β observed in

268 *Stim1*^{-/-} MEFs was substantially increased after HSV-1 infection (Fig. 6a). We also observed a
269 marked reduction in expression of GFP, encoded from the viral genome which served as an indicator
270 for viral replication in *Stim1*^{-/-} MEFs. We observed similar results using another DNA virus, MHV-68.
271 Similar to HSV-1 infection, MHV-68-infected *Stim1*^{-/-} MEFs showed much lower expression of the
272 viral genome-driven GFP, as well as early and late phase viral transcripts (e.g., *ORF57* and *ORF29*,
273 respectively), indicative of a lower viral burden (Fig. 6b). In consistence with these data, *Stim1*^{-/-}
274 MEFs showed enhanced phosphorylation of IRF3 upon HSV-1 infection (Fig. 6c). We observed
275 similar results in primary cells, where *Stim1*^{-/-} BMDMs showed enhanced expression of *Ifnb1* and *Il6*
276 mRNAs under resting conditions, as well as after HSV-1 infection (Fig. 6d). Together, these data
277 show that loss of STIM1 increases resistance to DNA virus infections.

278 Next, we validated these observations in *STIM1*^{-/-} THP1 macrophages. Similar to data with
279 mouse cells, STIM1 deficiency rendered human macrophages resistant to HSV-1, decreasing
280 expression of GFP as observed by microscopy and transcript analyses (Fig. 6e). Accordingly, we
281 observed enhanced expression of *IFNB1* transcripts in *STIM1*^{-/-} THP1 cells. Previously, it was shown
282 that anti-viral immunity against HIV infection also relies on the cGAS-STING pathway due to the
283 presence of cytosolic DNA generated by reverse-transcription^{8, 33}. To investigate whether STIM1
284 deletion imparts resistance to HIV, we infected wild type and *STIM1*^{-/-} THP1 cells with GFP-HIV and
285 observed a dramatic reduction of HIV infection in *STIM1*^{-/-} THP1 cells as judged by frequency of
286 GFP⁺ cells (Fig. 6f). Together, these results suggest that deficiency of STIM1 can prime host
287 response against infection with DNA viruses and retroviruses in various murine and human cell types.

288 Many DNA viruses, including HSV-1 are known to activate Ca²⁺ signaling for a productive
289 infection³⁴. Hence it is possible that resistance to DNA virus infection in *Stim1*^{-/-} MEFs may be due to
290 loss of SOCE. To determine the contribution of SOCE versus enhanced STING activity in host
291 resistance to DNA virus infection, we compared responses of *Stim1*^{-/-} and *Orai1*^{-/-} MEFs to HSV-1
292 infection. We observed a moderate resistance to HSV-1 infection in *Orai1*^{-/-} MEFs, but in comparison,
293 the resistance to HSV-1 infection was approximately 100-fold more pronounced in *Stim1*^{-/-} cells

294 (Supplementary Fig. 6a). In support of the SOCE-independent role of STIM1 in regulation of STING
295 function, we found that *Ifnb1* mRNA expression was not increased after HSV-1 infection in *Orai1*^{-/-}
296 cells contrary to *Stim1*^{-/-} cells. Finally, *Stim1*^{-/-} MEFs when treated with inhibitor of the IFN receptor-
297 JAK-STAT pathway, tofacitinib, became susceptible to HSV-1 infection (Supplementary Fig. 6b).
298 Together, these results indicate a predominant role of the type I IFN pathway in the resistance of
299 STIM1-deficient cells to viral infections.

300

301 **Ablation of STIM1 primes type I IFN response in vivo**

302 To gain insight into the importance of STIM1 in host defense against viral infection in vivo, we
303 investigated the antiviral immune response in *Stim1*^{fl/fl} and *Stim1*^{fl/fl}*Lyz2*-cre mice. In parallel, to
304 compare the contribution of SOCE in host resistance to viral infections, we generated conditionally
305 targeted *Orai1* animals (Supplementary Fig. 7a), which were bred with *Lyz2*-cre for two generations.
306 BMDMs differentiated from bone marrows of *Orai1*^{fl/fl}*Lyz2*-cre animals showed almost a complete loss
307 of *Orai1* transcripts and SOCE (Supplementary Fig. 7b, c). Since HSV-1 is a neurotropic virus and the
308 leading cause of sporadic viral encephalitis, we investigated the effects of *Orai1* and *Stim1* deficiency
309 on HSV-1-induced lethality and viral loads in the brain. When infected with HSV-1 intravenously,
310 control (*Stim1*^{fl/fl} and *Orai1*^{fl/fl}) as well as *Orai1*^{fl/fl}*Lyz2*-cre animals showed susceptibility and died
311 within 6-8 days of infection (Fig. 7a, b). In contrast *Stim1*^{fl/fl}*Lyz2*-cre mice were completely resistant to
312 HSV-1-induced lethality, and accordingly, recovered from loss of body weight. Viral titers in the brains
313 obtained from *Stim1*^{fl/fl}*Lyz2*-cre mice were significantly lower than *Stim1*^{fl/fl} animals (Fig. 7c).
314 Importantly, serum cytokine measurements showed elevated levels of serum IFN-β, IL-6 and TNF in
315 uninfected as well as HSV-1-infected *Stim1*^{fl/fl}*Lyz2*-cre mice, when compared to littermate controls
316 (Fig. 7d). Taken together, our data indicate that genetic deletion of *Stim1* but not *Orai1* can impart
317 protection from HSV-induced encephalitis and lethality, due to pre-activation of the STING-mediated
318 type I IFN signaling pathway.

319

320 Discussion

321 STING and STIM1 commonly contain transmembrane domain(s) in their N termini and predominantly
322 localize to the ER membrane. Co-immunoprecipitation experiments showed an association between
323 the two proteins, that was primarily mediated by their N-terminal transmembrane domains. We
324 showed that loss of STIM1 renders cells and mice strongly resistant to viral infections due to
325 enhanced expression of type I IFNs and pro-inflammatory cytokines. Importantly, a patient with a
326 mutation in *STIM1* that abrogated STIM1 expression also showed elevated cytokines and ISGs.
327 Furthermore, some of the patient's clinical features, principally the skin and nail manifestations
328 resemble that of SAVI patients, suggesting that the excessive type I IFNs do have adverse biological
329 manifestation in this condition²⁵. Mechanistically, enhanced translocation and dimerization of STING
330 by STIM1 deficiency suggest that STIM1 may preferentially bind to STING monomers at the ER to
331 prevent its spontaneous activation. Conversely, we also found that STING deficiency augmented
332 translocation of STIM1 and Ca²⁺ entry triggered by depletion of ER Ca²⁺ stores. Therefore, our studies
333 suggest that physical and functional association between STIM1 and STING is crucial for
334 maintenance of the resting state of both pathways.

335 We showed that enhanced type I IFN expression in STIM1-deficient cells is not mediated by
336 Ca²⁺ signaling by comparative studies with Orai1-deficient cells and animals. STIM1 deficiency made
337 cells and mice strongly resistant to HSV-1 infections. Since many viruses including HSV-1³⁴, require
338 elevated Ca²⁺ levels for their replication, we determined the contribution of the Ca²⁺-dependent (i.e.,
339 decreased SOCE) vs. Ca²⁺-independent mechanisms (i.e., enhanced type I IFN response) involved in
340 anti-viral immunity in STIM1-deficient cells using two independent molecular tools, *Orai1*^{-/-} cells/mice
341 and JAK inhibitors. These results suggest that decreased viral burden in STIM1-deficient cells and
342 mice is predominantly derived from enhanced type I IFN responses. Whether the same principle can
343 be applied to other viruses with various degrees of dependence on Ca²⁺ signaling and activation of
344 the STING pathway needs further studies.

345 Although much is understood regarding the mechanisms underlying activation of STING
346 including ligand binding, trafficking and interaction with downstream effector molecules, little is known
347 about regulation of its resting state. Multiple mechanisms underlying STING inhibition have been
348 uncovered due to the importance of timely inactivation of the type I IFN signaling pathway. NLRX1
349 and ATG9a have been shown to inhibit STING-TBK1 interaction^{26, 27}. In addition, K48-linked
350 polyubiquitination by RNF5 and TRIM30a results in STING degradation after ligand binding^{35, 36}. All
351 these inhibitory mechanisms target STING function after ligand binding and trafficking. However,
352 inhibition of STING trafficking by brefeldin A, an inhibitor of ADP ribosylation factor (ARF) GTPases,
353 blocks activation of the downstream pathway, suggesting that trafficking of STING is crucial for its
354 function¹⁴. Consistently, our studies reveal a novel mechanism of regulation of STING activity,
355 inhibition of STING trafficking via direct interaction with STIM1. Activity of three of the disease-
356 associated STING variants; V147L, N154S, and V155M was suppressed by STIM1 in part via
357 blocking their translocation to the ERGIC, demonstrating a therapeutic potential of our finding. In
358 summary, our study identifies STIM1 as an “ER retention factor” to maintain ER residency and
359 inactive conformation of STING. Further, it suggests that one of the primary functions of CDN binding
360 to STING is to disrupt its association with STIM1 that would allow exit of STING from the ER. Further
361 dissection of the mechanisms underlying maintenance of the resting state of STING may inform the
362 design of specific therapeutic strategies geared towards enhancement/inhibition of STING activity in
363 the context of vaccination and sterile inflammatory diseases (e.g., AGS and SAVI), respectively.

364

365 **Methods**

366 **Chemicals and Antibodies.** Fura 2-AM (F1221) was purchased from ThermoFisher Scientific.
367 Thapsigargin and ionomycin were purchased from EMD Millipore. Poly(I:C) (P1530) was purchased
368 from Millipore Sigma. Poly(dA:dT) (tlrl-patn) and 2',3'-cGAMP (tlrl-nacga23) were purchased from
369 InvivoGen. Tofacitinib (S500110MG) was purchased from Selleck Chemical LLC. Antibodies for
370 detection of STIM1 (5668S), phosphor-IRF3 (29047S), IRF3 (4302S), phosphor-TBK1 (5483S), total

371 TBK1 (3504S), STING (13647S), 6xHis tag (12698S), and STIM2 (4917S) were purchased from Cell
372 Signaling Technologies. Antibodies for detection of FLAG tag (F3040), p58 (ERGIC marker, E1031)
373 and human Orai1 (AB9868) were purchased from Millipore Sigma. Antibody for detection of β -actin
374 (sc-47778) was obtained from Santa Cruz Biotechnology and antibodies for detection of STIM1 (clone
375 5A2) and GAPDH (GTX100118) from human PBMCs were obtained from Sigma and GeneTex
376 respectively.

377 **Plasmids and cells.** STIM1-YFP plasmid has been described previously³⁷. Human STIM1 cDNA was
378 subcloned into a lentiviral vector, FGLIF (kind gift from Dr. Dong Sun An, UCLA) with a C-terminal
379 FLAG tag and pcDNA 3.1 mychis plasmid. GST-tagged truncated fragments of STIM1 corresponding
380 to amino acids 1-249 (containing the EF-hand, SAM domain and transmembrane segment), 250–400
381 (containing coiled-coil domains 1 and 2), the CAD domain (amino acids 342–448), 400–600 (the
382 serine and threonine-rich region), and 600–685 (the C-terminal PIP₂-interacting domain) have been
383 previously described³⁷. Fragments of STING corresponding to the N-terminal TM domain (a.a. 1-154)
384 and C-terminal domain (a.a. 149-379), both tagged with a FLAG tag in the C-terminus, were
385 subcloned into pMSCV-CITE-eGFP-PGK-Puro vector. Full-length cDNA of human STING and SAVI
386 mutants corresponding to V147L, N154S and V155M were subcloned into pEGFPN1 vector to
387 generate a C-terminal GFP fusion protein and into pMSCV-CITE-eGFP-PGK-Puro vector that
388 encodes a C-terminal FLAG tag using primers described in Supplementary Table 1. Oligonucleotides
389 encoding sgRNAs to delete *STIM1*, *STIM2* and *STING* were subcloned into lentiGuide-Puro vector
390 (Addgene, #52963). HEK293T, Vero and Jurkat E6-1 T cell lines were obtained from American Type
391 Culture Collection center (ATCC, Manassas, VA). WT and *Stim1*^{-/-} MEFs were generated by breeding
392 *Stim1*^{fl/fl} mice (Jackson Laboratory, stock No. 023350) with *CMV*-cre mice (Jackson Laboratory, stock
393 No. 006054). MEFs were established using standard protocols from E14.5 embryos and retrovirally
394 transduced with SV40 large T antigen in a plasmid encoding hygromycin resistance for
395 immortalization. *Orai1*^{-/-} MEFs have been previously described³⁸.

396 **Cell Culture.** MEFs, Vero and HEK293T cells were grown in complete DMEM (Mediatech)

397 supplemented with 10% (v/v) fetal bovine serum (Hyclone), 2 mM L-glutamine (Mediatech), 10 mM
398 HEPES (Mediatech) and Penicillin/Streptomycin (Mediatech) at 37 C and 5% CO₂. BMDMs were
399 differentiated from bone marrow cells isolated from femur and tibia of 6-8-week-old mice. For
400 preparation of BMDMs, the bone marrow cells were cultured in 10% M-CSF-containing conditional
401 medium from HEK293T cells expressing recombinant M-CSF (a kind gift from Stephen Smale lab,
402 UCLA) for 4-6 days. BMDMs were cultured in the absence of M-CSF for at least 24 hours prior to
403 experimental use. THP1 and Jurkat T cells were cultured in RPMI (Mediatech) containing 10% fetal
404 bovine serum (Hyclone). Cells were infected with indicated MOIs of indicated viruses and harvested in
405 TRIzol Reagent for transcript expression analysis. For 2',3'-cGAMP treatment, MEFs or HEK293T
406 cells were treated with or without 1 μM 2',3'-cGAMP for 30 mins in digitonin permeabilization buffer
407 (50 mM HEPES, 100 mM KCl, 3 mM MgCl₂, 0.1 mM DTT, 85 mM sucrose, 0.2% BSA, 1 mM ATP, 0.1
408 mM GTP, pH 7.0) followed by culture medium for indicated times, after which the cells were harvested
409 for transcript analysis or reporter assays. MEFs were transfected with 5 μg of interferon stimulatory
410 DNA (ISD³⁹), polydA:dT or poly I:C using Lipofectamine 2000 (Thermofisher Scientific). For ELISAs,
411 MEFs were treated with cGAMP as described and supernatant harvested after 24 hrs.

412 **Mice.** *Stim1^{fl/fl}* animals were purchased from Jackson Laboratory (stock No. 023350) and bred with
413 *Lyz2-cre* animals (Jackson Laboratory, stock No. 004781) for two generations. Targeting of murine
414 *Orai1* was performed by flanking exon 2 with LoxP sites by homologous recombination in AB2.2
415 (129SvEv) embryonic stem (ES) cells. Exon 2 encodes for 201 a.a. out of a total of 304 a.a. of Orai1
416 protein. G418-resistant clones were screened by PCR for homologous recombination at both
417 homology arms. Chimeric mice with floxed *Orai1* alleles were generated by blastocyst injection of
418 heterozygous *Orai1^{fl/+}* ES cell clones. Founder *Orai1^{fl/+}* mice were bred with Flp-deleter mice (Jackson
419 Laboratory) to remove the neomycin resistance gene cassette. *Orai1^{fl/fl}* mice were backcrossed to
420 C57/BL6/J mice for at least 10 generations and then bred with *Lyz2-cre* mice to generate myeloid-
421 specific deletion of *Orai1*. All mice were maintained in pathogen-free barrier facilities and used in
422 accordance with protocols approved by the Institutional Animal Care and Use Committee at the

423 UCLA.

424 **Patient.** Sample collection from the patient was performed after obtaining written consent from his
425 parents according to the principles of the Declaration of Helsinki and after local ethics approval.
426 Detailed clinical evaluation was undertaken in appropriate clinical setting. PBMC isolation from
427 healthy control and patient human blood samples was performed by gradient separation using
428 Lymphoprep (Stem Cell Technologies). Monocytes were purified from PBMCs using a Monocytes
429 separation kit II (# 130-091-153, Miltenyi Biotec). The patient is a 4-year-old boy of consanguineous
430 Pakistani background, who initially presented to paediatric neurology due to poor mobility. A diagnosis
431 of STIM1 deficiency was made following referral to paediatric immunology due to recurrent
432 sinopulmonary infections. The patient has typical non-immunological features consistent with STIM1
433 deficiency including amelogenesis imperfecta resulting in complete dental clearance, anhidrosis and
434 muscle weakness. Surprisingly, the patient had mild immunodeficiency phenotype, with relatively
435 preserved immunological function, including appropriate responses to challenge vaccination²⁵.

436 **Virus amplification and concentration.** MHV68-GFP virus was amplified and titrated in NIH3T3
437 cells using standard protocols. HSV-1 KOS strain was used for all in vitro experiments and HSV-1 17+
438 strain was used for in vivo infection experiments. Both the strains were amplified and titrated in Vero
439 cells using standard protocols. HSV-1 17+ strain was concentrated for in vivo experiments. VSV-G
440 pseudotyped HIV-1_{NL4-3} strain-GFP reporter virus was amplified and titrated in HEK293T cells using
441 standard protocols.

442 **RNA isolation, cDNA synthesis and Real-time quantitative PCR.** Total RNA from cells harvested
443 in TRIzol Reagent (ThermoFisher) was isolated using the Direct-zol RNA isolation kit (Zymo
444 Research). RNA quantity and quality were confirmed with a NanoDrop ND-1000 spectrophotometer.
445 cDNA was synthesized using 2-3 µg of total RNA using oligo(dT) primers and Maxima Reverse
446 Transcriptase (Thermofisher Scientific). Real-time quantitative PCR was performed using iTaq
447 Universal SYBR Green Supermix (Bio-Rad) and an iCycler IQ5 system (Bio-Rad) using gene-specific
448 primers described in Supplementary Table 1. Threshold cycles (C_T) for all the candidate genes were

449 normalized to those for *36b4* to obtain ΔC_T and further normalized to the values obtained for WT
450 samples to obtain $\Delta\Delta C_T$. The specificity of primers was examined by melt-curve analysis and agarose
451 gel electrophoresis of PCR products. Total RNA from human patient and healthy donors PBMCs and
452 monocytes harvested was isolated using the Total RNA purification Kit (Norgen Biotek Corp.). cDNA
453 was synthesized using 1-2 μ g of total RNA using High-Capacity cDNA Reverse Transcription Kit
454 (ThermoFisher Scientific). Real-time quantitative PCR was performed using TaqMan Universal PCR
455 Master Mix (ThermoFisher Scientific) using FAM-MGB probes for detection of *MX1*
456 (Hs00895608_m1), *IFI44* (Hs00951349), *IFI44L* (Hs00915292_m1), *IFI27* (Hs01086370_m1), *ISG15*
457 (Hs00192713_m1), *CXCL10* (Hs01124251_g1), *RSAD2* (Hs01057264_m1), *IFIT1* (Hs01675197_m1),
458 *IFI6* (Hs00242571_m1), *OAS1* (Hs00973635_m1), *IL6* (Hs00985639_m1), and *HPRT1*
459 (Hs99999909_m1). The relative abundance of each transcript was normalized to the expression level
460 of *HPRT1* to obtain ΔC_T and further normalized to the values obtained for healthy controls to obtain
461 $\Delta\Delta C_T$.

462 **Cytokine measurement by ELISA.** ELISA was performed on cell culture supernatants from indicated
463 cells or serum samples harvested from mock or HSV-1-infected animals for detection of IFN β
464 (Biolegend, # 439407), IL-6 (ThermoFisher, # 88-7064-88) and TNF (ThermoFisher, # 88-7324-88).
465 Serum samples obtained from healthy controls or STIM1-deficient human patient were used for
466 detection of IFN β (PBL Assay Science, #41410), IL-6 (ThermoFisher Scientific, # 88-7066-22) and
467 TNF (ThermoFisher Scientific, # 88-7346-22).

468 **Single-cell Ca²⁺ imaging, live-cell epifluorescence or TIRF microscopy and confocal**
469 **microscopy.** THP1 and Jurkat T cells were loaded at 1 x 10⁶ cells/ml with 1 μ M Fura 2-AM for 40 min
470 at 25°C and attached to poly-L-lysine-coated coverslips. MEFs or BMDMs were grown overnight on
471 coverslips and loaded with 1 μ M Fura 2-AM for 40 min at 25°C for imaging. Intracellular [Ca²⁺]_i
472 measurements were performed using essentially the same methods as previously described⁴⁰. For
473 live-cell epifluorescence imaging of STING-GFP translocation kinetics, MEFs grown on coverslips
474 were perfused with Ringer's solution containing (in mM): 155 NaCl, 4.5 KCl, 2 CaCl₂, 1 MgCl₂, 10 D-

475 glucose, and 5 Na-HEPES (pH 7.4) and used for time course imaging. Cells were perfused with
476 digitonin permeabilization buffer (50 mM HEPES, 100 mM KCl, 3 mM MgCl₂, 0.1 mM DTT, 85 mM
477 sucrose, 0.2% BSA, 1 mM ATP, 0.1 mM GTP, pH 7.0) containing 1 μM 2',3'-cGAMP for 10 mins and
478 then the medium was replaced with Ringer's solution. For TIRF analysis of STIM1-YFP translocation,
479 MEFs were plated onto coverslip bottom dishes in medium and used for experiments. Medium was
480 replaced with Ringer's solution and cells were treated with 1 μM thapsigargin for passive depletion of
481 ER Ca²⁺ stores to monitor STIM1 translocation. TIRF microscopy was performed using an Olympus
482 IX2 illumination system mounted on an Olympus IX51 inverted microscope using previously described
483 methods³⁷. Acquisition and image analysis were performed using Slidebook (Intelligent Imaging
484 Innovations, Inc.) software and graphs were plotted using OriginPro8.5 (Originlab). For quantification
485 of TIRF intensity across different cells, individual regions of interest were selected and data were
486 analyzed as the ratio of fluorescence intensity at each time-point (F) to that at the start of the
487 experiment (F₀). For confocal analysis, uninfected or HSV-infected MEFs were fixed for 20 mins with
488 2.5% PFA at room temperature, permeabilized in buffer containing PBS + 0.2% Triton X-100, blocked
489 with same buffer containing 1% BSA and used for staining of ERGIC marker and confocal analysis.
490 Confocal laser scanning microscopy was performed using Fluoview FV10i Confocal Microscope
491 (Olympus), images were captured with a 60x oil objective. Images were processed for enhancement
492 of brightness or contrast using Fluoview software.

493 **Generation of STIM1, STIM2 and STING-deficient cells using CRISPR-Cas9 system.** To generate
494 lentiviruses for transduction, HEK293T cells were transfected with plasmid(s) encoding sgRNA and
495 packaging vectors (pMD2.G and psPAX2, Addgene) using calcium phosphate transfection method.
496 Lentiviruses encoding Cas9 were generated using the same technique. Culture supernatants were
497 harvested at 48 and 72 hours post transfection and used for infection (50% of Cas9-encoding virus +
498 50% of sgRNA-encoding virus) of MEFs, THP1 or Jurkat T cells together with polybrene (8 μg/ml)
499 using the spin-infection method. Cells were selected with puromycin (1 μg/ml) and blasticidin (5 μg/ml)
500 48 hours post infection. The sequences of the sgRNAs are described in Supplementary Table 1.

501 **Immunoprecipitation and immunoblotting.** For immunoprecipitation, cDNA encoding full-length or
502 fragments (a.a. 1-154 and 149-379) of FLAG-tagged STING and 6xHis-tagged STIM1 was transfected
503 into HEK293T cells. Transfected cells (2×10^7) were lysed in lysis buffer (20 mM Tris-Cl, 2 mM EDTA,
504 135 mM NaCl, 10% (vol/vol) glycerol, 0.5% Igepal CA-630, protease inhibitor mixture, pH 7.5) and
505 centrifuged at 100,000 x g for 1 hour before preclearing with protein G-Sepharose. Lysates were
506 immunoprecipitated with anti-FLAG antibody-conjugated resin for 6 hours. Immunoprecipitates were
507 washed five times in lysis buffer and analyzed by immunoblotting. For immunoblot analyses, cells
508 were lysed in RIPA buffer (10 mM Tris-Cl, 1% Triton X-100, 0.1% SDS, 140 mM NaCl, 1 mM EDTA,
509 0.1% sodium deoxycholate, and cComplete Protease Inhibitor Cocktail [Sigma-Aldrich], pH 8.0) and
510 centrifuged to remove debris. Samples were separated on 8-10% SDS-PAGE. Proteins were
511 transferred to nitrocellulose membranes and subsequently analyzed by immunoblotting with relevant
512 antibodies. For dithiobis succinimidyl propionate (DSP) crosslinking, MEFs or HEK293T cells were left
513 untreated or treated with 0.125, 0.25, 0.5, or 1.0 mM of DSP for 1 hour on ice, followed by quenching
514 with 20 mM Tris-Cl, pH 7.5. Cells were lysed in SDS loading dye under non-reducing conditions
515 (without β -Mercaptoethanol) and separated on 10% SDS-PAGE and immunoblotted for detection of
516 indicated proteins. For endogenous immunoprecipitation, HEK293 cells were lysed in lysis buffer
517 (same as above) and centrifuged at 100,000 x g for 1 hour before preclearing with protein G-
518 Sepharose. Lysates were incubated with 2 μ g of anti-STING antibody (Cell Signaling Technologies)
519 overnight and subsequently with protein G-Sepharose for 2 hours. For immunoprecipitation of STING
520 SAVI mutants with endogenous STIM1, HEK293T stably expressing FLAG-tagged human STING^{WT},
521 STING^{V147M}, STING^{N154S} or STING^{V155M} cDNAs were lysed in lysis buffer (same as above), centrifuged
522 at 100,000 x g for 1 hour, pre-cleared and incubated with anti-FLAG antibody-conjugated resin
523 overnight in lysis buffer containing 0.1% Igepal CA-630 and processed as described above. PBMCs
524 were lysed in NP40 Lysis Buffer (VWR Life Science) containing cComplete Protease Inhibitor Cocktail
525 (Sigma-Aldrich) and centrifuged to remove debris. 20 μ g of total protein from healthy control or patient
526 samples was separated on a 4-12% Bis-Tris Plus Gel (ThermoFisher), transferred to polyvinylidene
527 difluoride (PVDF) membrane and subsequently analyzed by immunoblotting with relevant antibodies.

528 **Purification of recombinant proteins from *E. coli*.** Full-length and fragments (a.a. 1-249, 250-400,
529 324-448, 400-600, and 600-685) of STIM1 were subcloned into pGEX4T-1 plasmid. GST fusion
530 protein expressing transformants were grown in liquid cultures and induced with isopropyl-1-thio- β -D-
531 galactopyranoside (IPTG, 0.2 mM) at 18 C overnight. Subsequently, cells were harvested and
532 resuspended in lysis buffer (50 mM NaH₂PO₄, 500 mM NaCl, 10% glycerol, pH 8.0) containing
533 protease inhibitors and 0.5% Triton X-100. Lysates were sonicated, centrifuged to remove debris and
534 incubated with glutathione sepharose 4B beads for 2 hrs. After washing 8 times with lysis buffer, the
535 beads were stored in lysis buffer without Triton X-100 at -20°C.

536 **GST pulldown analysis.** cDNA encoding full-length and fragments of STING-FLAG was transfected
537 into HEK293T cells. Transfected cells (2×10^7) were lysed in lysis buffer (20 mM Tris-Cl, 2 mM EDTA,
538 135 mM NaCl, 10% (vol/vol) glycerol, 0.5% Igepal CA-630, protease inhibitor mixture, pH 7.5) and
539 centrifuged at 100,000 x g for 1 hour before preclearing with protein G-Sepharose. Lysates were
540 incubated with 20 μ g of GST or GST-tagged fragments of STIM1 for 18 hours in binding buffer (0.5%
541 Igepal CA-630, 20 mM Tris-HCl, 100 mM NaCl, 2 mM EDTA, 10% glycerol, protease inhibitors, pH
542 7.5). Pulldown samples were washed five times with lysis buffer and analyzed by immunoblotting for
543 indicated proteins.

544 **HSV infection in mice.** Age and gender-matched control (*Stim1^{fl/fl}* or *Orai1^{fl/fl}*), *Stim1^{fl/fl}Lyz2-cre* or
545 *Orai1^{fl/fl}Lyz2-cre* mice were intravenously injected with 1×10^7 pfu of HSV-1 17+ strain. The viability of
546 the infected mice was monitored for 10 days. Mouse serum was collected at indicated times after
547 infection for measurement of serum cytokine by ELISA.

548 **Statistical analysis.** Statistical analysis was performed using the Origin2018b software (OriginLab,
549 Northampton, MA, USA). Data are presented as mean \pm s.e.m. For all dataset, normality and
550 homogeneity of variance were evaluated by Shapiro-Wilk test and Levene test respectively, to ensure
551 that the assumptions inherent to parametric significance testing were not violated. Statistical
552 significance to compare two quantitative groups was evaluated using two-tailed/unpaired t-test. When
553 multiple groups and/or multiple condition comparisons were necessary, one-way or two-way ANOVA

554 was performed followed by a Tukey HSD post-hoc test. Statistical comparison of multiple counts in
555 contingency tables was performed using Chi-square test followed by pairwise analysis of differences
556 as post-hoc test. A critical value for significance of $P < 0.05$ was used throughout the study, and
557 statistical thresholds of 0.05, 0.005 as well as 0.0005 are indicated in the figures by asterisks (see
558 legends for details).

559

560 **Data availability**

561 The data that support the findings of this study are available from the corresponding authors upon
562 request. The manuscript describing clinical phenotype of *STIM1* patient is available from OSR
563 Preprints (<https://doi.org/10.31219/osf.io/4duxt>).

564

565 **References**

- 566 37. Srikanth, S. *et al.* A novel EF-hand protein, CRACR2A, is a cytosolic Ca²⁺ sensor that
567 stabilizes CRAC channels in T cells. *Nat Cell Biol* **12**, 436-446 (2010).
- 568
- 569 38. Gwack, Y. *et al.* Hair loss and defective T- and B-cell function in mice lacking ORAI1. *Mol Cell*
570 *Biol* **28**, 5209-5222 (2008).
- 571
- 572 39. Stetson, D.B. & Medzhitov, R. Recognition of cytosolic DNA activates an IRF3-dependent
573 innate immune response. *Immunity* **24**, 93-103 (2006).
- 574
- 575 40. Srikanth, S., Jung, H.J., Ribalet, B. & Gwack, Y. The intracellular loop of Orai1 plays a central
576 role in fast inactivation of Ca²⁺ release-activated Ca²⁺ channels. *J Biol Chem* **285**, 5066-5075
577 (2010).

578

579 **ACKNOWLEDGEMENTS**

580 We thank Dr. S. Bensinger (UCLA) for sharing THP1 cells, Drs. X. Liu and S. Smale (UCLA) for
581 BMDM differentiation protocols and reagents. We thank Drs. N-H. Park, K-H. Shin, M. K. Kang, R.
582 Kim, Y. Wang and T. M. Vondriska (UCLA) for sharing their confocal imaging facilities. We thank Dr.

583 J-L. Casanova (Rockefeller University) for providing STIM1 patient B cell line. This work was
584 supported by the National Institute of Health grants AI083432 and DE028432 (Y.G.) and AI130653
585 (S.S.). This work was also supported in part by CA180779, CA200422, AI073099, AI116585,
586 AI129496, AI140705, DE023926, DE027888, Fletcher Jones Foundation, and Whittier Foundation
587 (J.U.J.).

588

589 **AUTHOR CONTRIBUTIONS**

590 Y.G. and S.S. designed research; S.S. performed all the in vitro experiments using MEFs, THP1 and
591 BMDMs with technical help from J.L.; J.S.W. performed biochemical experiments of interaction
592 between STIM1 and STING, SAVI mutant analyses, and in vivo HSV infection experiments with help
593 from B.W.; Y.E, L.R and S.Savic collected and analyzed patient samples together with S.S and
594 J.S.W.; K.C. and D.S.A. performed the HIV infection experiments; G.J.S. and J.U.J. provided reagents
595 and protocols for in vitro HSV infections; R.C. and E.C. provided reagents and protocols for in vivo
596 HSV infections; T.T.W. and R.S. provided reagents and protocols for MHV-68 infections; G.C. helped
597 with statistical analysis; S.S. and Y.G. wrote the manuscript with input from all authors and supervised
598 the project.

599

600 **COMPETING INTERESTS**

601 The authors do not have any competing financial interests.

602

603 **References**

604

605 1. Ishikawa, H. & Barber, G.N. STING is an endoplasmic reticulum adaptor that facilitates innate
606 immune signalling. *Nature* **455**, 674-678 (2008).

607

608 2. Zhong, B. *et al.* The adaptor protein MITA links virus-sensing receptors to IRF3 transcription
609 factor activation. *Immunity* **29**, 538-550 (2008).

610

611 3. Sun, W. *et al.* ERIS, an endoplasmic reticulum IFN stimulator, activates innate immune
612 signaling through dimerization. *Proc Natl Acad Sci U S A* **106**, 8653-8658 (2009).

613

614 4. Barber, G.N. STING: infection, inflammation and cancer. *Nat Rev Immunol* **15**, 760-770
615 (2015).

616

617 5. Chen, Q., Sun, L. & Chen, Z.J. Regulation and function of the cGAS-STING pathway of
618 cytosolic DNA sensing. *Nat Immunol* **17**, 1142-1149 (2016).

619

620 6. Li, T. & Chen, Z.J. The cGAS-cGAMP-STING pathway connects DNA damage to
621 inflammation, senescence, and cancer. *J Exp Med* (2018).

622

623 7. Li, Y., Wilson, H.L. & Kiss-Toth, E. Regulating STING in health and disease. *J Inflamm (Lond)*
624 **14**, 11 (2017).

625

626 8. Yan, N., Regalado-Magdos, A.D., Stiggelbout, B., Lee-Kirsch, M.A. & Lieberman, J. The
627 cytosolic exonuclease TREX1 inhibits the innate immune response to human
628 immunodeficiency virus type 1. *Nat Immunol* **11**, 1005-1013 (2010).

629

630 9. Ahn, J., Gutman, D., Saijo, S. & Barber, G.N. STING manifests self DNA-dependent
631 inflammatory disease. *Proc Natl Acad Sci U S A* **109**, 19386-19391 (2012).

632

633 10. Crow, Y.J. & Manel, N. Aicardi-Goutieres syndrome and the type I interferonopathies. *Nat Rev*
634 *Immunol* **15**, 429-440 (2015).

635

636 11. Liu, Y. *et al.* Activated STING in a vascular and pulmonary syndrome. *N Engl J Med* **371**, 507-
637 518 (2014).

638

639 12. Melki, I. *et al.* Disease-associated mutations identify a novel region in human STING
640 necessary for the control of type I interferon signaling. *J Allergy Clin Immunol* **140**, 543-552
641 e545 (2017).

642

643 13. Jeremiah, N. *et al.* Inherited STING-activating mutation underlies a familial inflammatory
644 syndrome with lupus-like manifestations. *J Clin Invest* **124**, 5516-5520 (2014).

- 645
646 14. Dobbs, N. *et al.* STING Activation by Translocation from the ER Is Associated with Infection
647 and Autoinflammatory Disease. *Cell Host Microbe* **18**, 157-168 (2015).
- 648
649 15. Zhang, X. *et al.* Cyclic GMP-AMP containing mixed phosphodiester linkages is an endogenous
650 high-affinity ligand for STING. *Mol Cell* **51**, 226-235 (2013).
- 651
652 16. Prakriya, M. & Lewis, R.S. Store-Operated Calcium Channels. *Physiol Rev* **95**, 1383-1436
653 (2015).
- 654
655 17. Feske, S., Skolnik, E.Y. & Prakriya, M. Ion channels and transporters in lymphocyte function
656 and immunity. *Nat Rev Immunol* **12**, 532-547 (2012).
- 657
658 18. Baba, Y. & Kurosaki, T. Role of Calcium Signaling in B Cell Activation and Biology. *Curr Top*
659 *Microbiol Immunol* **393**, 143-174 (2016).
- 660
661 19. Srikanth, S., Woo, J.S., Sun, Z. & Gwack, Y. Immunological Disorders: Regulation of Ca(2+)
662 Signaling in T Lymphocytes. *Adv Exp Med Biol* **993**, 397-424 (2017).
- 663
664 20. Lacruz, R.S. & Feske, S. Diseases caused by mutations in ORAI1 and STIM1. *Ann N Y Acad*
665 *Sci* **1356**, 45-79 (2015).
- 666
667 21. Notarangelo, L.D., Kim, M.S., Walter, J.E. & Lee, Y.N. Human RAG mutations: biochemistry
668 and clinical implications. *Nat Rev Immunol* **16**, 234-246 (2016).
- 669
670 22. Brandman, O., Liou, J., Park, W.S. & Meyer, T. STIM2 is a feedback regulator that stabilizes
671 basal cytosolic and endoplasmic reticulum Ca²⁺ levels. *Cell* **131**, 1327-1339 (2007).
- 672
673 23. Soboloff, J., Rothberg, B.S., Madesh, M. & Gill, D.L. STIM proteins: dynamic calcium signal
674 transducers. *Nat Rev Mol Cell Biol* **13**, 549-565 (2012).
- 675
676 24. Picard, C. *et al.* STIM1 mutation associated with a syndrome of immunodeficiency and
677 autoimmunity. *N Engl J Med* **360**, 1971-1980 (2009).
- 678
679 25. Rice, A. *et al.* A report of novel STIM1 deficiency and 6 year follow up of two previous cases
680 associated with mild immunological phenotype. [doi:10.31219/osf.io/4duxt](https://doi.org/10.31219/osf.io/4duxt) (2018).
- 681
682 26. Guo, H. *et al.* NLRX1 Sequesters STING to Negatively Regulate the Interferon Response,
683 Thereby Facilitating the Replication of HIV-1 and DNA Viruses. *Cell Host Microbe* **19**, 515-528
684 (2016).
- 685
686 27. Saitoh, T. *et al.* Atg9a controls dsDNA-driven dynamic translocation of STING and the innate
687 immune response. *Proc Natl Acad Sci U S A* **106**, 20842-20846 (2009).

- 688
689 28. Lau, L., Gray, E.E., Brunette, R.L. & Stetson, D.B. DNA tumor virus oncogenes antagonize the
690 cGAS-STING DNA-sensing pathway. *Science* **350**, 568-571 (2015).
- 691
692 29. Yuan, J.P. *et al.* SOAR and the polybasic STIM1 domains gate and regulate Orai channels.
693 *Nat Cell Biol* **11**, 337-343 (2009).
- 694
695 30. Ishikawa, H., Ma, Z. & Barber, G.N. STING regulates intracellular DNA-mediated, type I
696 interferon-dependent innate immunity. *Nature* **461**, 788-792 (2009).
- 697
698 31. Mukai, K. *et al.* Activation of STING requires palmitoylation at the Golgi. *Nat Commun* **7**,
699 11932 (2016).
- 700
701 32. Ouyang, S. *et al.* Structural analysis of the STING adaptor protein reveals a hydrophobic dimer
702 interface and mode of cyclic di-GMP binding. *Immunity* **36**, 1073-1086 (2012).
- 703
704 33. Gao, D. *et al.* Cyclic GMP-AMP synthase is an innate immune sensor of HIV and other
705 retroviruses. *Science* **341**, 903-906 (2013).
- 706
707 34. Cheshenko, N. *et al.* Herpes simplex virus triggers activation of calcium-signaling pathways. *J*
708 *Cell Biol* **163**, 283-293 (2003).
- 709
710 35. Zhong, B. *et al.* The ubiquitin ligase RNF5 regulates antiviral responses by mediating
711 degradation of the adaptor protein MITA. *Immunity* **30**, 397-407 (2009).
- 712
713 36. Wang, Y. *et al.* TRIM30alpha Is a Negative-Feedback Regulator of the Intracellular DNA and
714 DNA Virus-Triggered Response by Targeting STING. *PLoS Pathog* **11**, e1005012 (2015).
- 715
716
717
718
719

720 **Figure Legends**

721 **Figure 1. STIM1 deficiency spontaneously induces type I IFN response in murine and human**
722 **cells. a**, Representative immunoblot showing expression of STIM1 in wild type (WT) and *Stim1*^{-/-}
723 MEFs (left). qPCR analysis of indicated cytokines and ISGs in unstimulated indicated MEFs (right).
724 qPCR data show pooled technical replicates from two independent experiments (*Ifnb1* and *Il6*) and
725 one representative triplicate from two independent experiments (other genes). **b**, Levels of secreted
726 IFN-β from culture supernatants of unstimulated WT or *Stim1*^{-/-} MEFs. **c**, Representative traces
727 showing averaged SOCE from WT (31 cells), *Orai1*^{-/-} (30 cells) and *Stim1*^{-/-} (29 cells) MEFs after
728 passive depletion of intracellular Ca²⁺ stores with 1 μM thapsigargin (TG) in the presence of external
729 solution containing 20 mM Ca²⁺ (left). Bar graph (middle) shows averaged baseline subtracted SOCE
730 (± s.e.m.) from four independent experiments. right: qPCR analysis of *Ifnb1* mRNA in indicated MEFs.
731 **d**, Representative immunoblot showing expression of STIM1 in BMDMs (left). qPCR analysis of *Ifnb1*
732 and *Il6* mRNA in unstimulated WT and *Stim1*^{-/-} BMDMs (right). **e**, Immunoblot showing expression of
733 STIM1 in wild type (WT) and *STIM1*^{-/-} THP1 cells generated using two independent sgRNAs (sg#2)
734 and 3 (sg#3). qPCR analysis of *IFNB1* and *IL6* mRNA in unstimulated WT, *STIM1*^{-/-} THP1 cells and
735 those reconstituted for expression of STIM1 (right two panels). **f**, Secreted IFN-β levels from culture
736 supernatants of untreated or PMA-differentiated WT or *STIM1*^{-/-} THP1 cells. Data show
737 representative triplicate from two independent experiments (panels **b**, **e** and **f**) or pooled technical
738 replicates from two (**c**) or three (**d**) independent experiments. All immunoblot data (panels **a**, **d** and **e**)
739 are representative of three independent experiments with similar results. Data are shown as mean ±
740 s.e.m. *p < 0.005, and **p < 0.0005 (unpaired/two-tailed *t* test – a, b, d; One-way ANOVA – c; and
741 Two-way ANOVA – e).

742

743 **Figure 2. STING-TBK1-IRF3 pathway links loss of STIM1 expression to *Ifnb1* transcription. a**,
744 qPCR analysis of *Ifnb1* mRNA in indicated MEFs under resting conditions or after stimulation with
745 2',3'-cGAMP for 2 or 4 h (left). Numbers on top indicate average fold change relative to WT MEFs.

746 Secreted IFN- β levels from culture supernatants of indicated MEFs after stimulation with 2',3'-cGAMP
747 (right). Data show pooled technical replicates from two independent experiments (qPCR) or one
748 representative triplicate from two independent experiments (ELISA) with similar results. **b**, qPCR
749 analysis of *Irfb1* transcripts in indicated MEFs transfected with interferon stimulatory DNA (ISD),
750 poly(dA:dT) or poly (I:C) for indicated time (left). qPCR analysis of *IFNB1* mRNA from untreated or
751 indicated nucleic acid-transfected THP1 cells. **c**, Representative confocal images showing localization
752 of GFP-IRF3 in indicated MEFs. Bar graph below depicts quantification from indicated number of
753 cells. Scale bars, 5 μ m. **d**, Representative immunoblot for detection of IRF3 under non-reducing
754 conditions in DSP-crosslinked indicated MEFs, (left). Bar graph (right) shows densitometry analysis of
755 IRF3 ratio (dimer/monomer) from three independent experiments. **e**, Representative immunoblots
756 showing expression of phospho-TBK1 (P-TBK1), total TBK1, and β -actin from indicated cells.
757 Numbers below indicate normalized fold change in ratio of P-TBK1/total TBK1. **f**, Representative
758 immunoblots showing expression of STIM1 and STING in WT, *Stim1*^{-/-}, or *Stim1*^{-/-} and *Tmem173*^{-/-}
759 double knock out (DKO) MEFs (left). Expression of *Irfb1* and *Il6* transcripts in indicated MEFs under
760 resting conditions (left two panels) or 4 h after stimulation with 2',3'-cGAMP (right two panels). **g**,
761 Secreted IFN- β levels from culture supernatants of indicated MEFs after stimulation with indicated
762 nucleic acids. **h**, Representative immunoblots showing expression of STIM1 and STING in WT,
763 *STIM1*^{-/-}, *TMEM173*^{-/-} or *STIM1*^{-/-} and *TMEM173*^{-/-} double knock out (DKO) THP1 cells (left).
764 Representative traces of averaged SOCE from WT (33 cells), *STIM1*^{-/-}, (30 cells), *TMEM173*^{-/-} (31
765 cells) and DKO (31 cells) THP1 cells after passive depletion of intracellular Ca²⁺ stores with 1 μ M
766 thapsigargin (TG) in the presence of external solution containing 2 mM Ca²⁺ (middle). Bar graph
767 shows averaged baseline subtracted SOCE (\pm s.e.m.) from three independent experiments. Right
768 panels show qPCR analysis of *IFNB1* or *IL6* mRNA in indicated THP1 cells. Data show representative
769 triplicates from two independent experiments with similar results (**b**, **d**, **f**, **g** and **h**) unless indicated. All
770 immunoblots are representative of at least three independent experiments with similar results. Data
771 are shown as mean \pm s.e.m. *p < 0.05, **p < 0.005, ***p < 0.0005 [Two-way ANOVA – a (left panel);
772 unpaired/two-tailed *t* test – a (right panel), b; Chi-square test – c; and One-way ANOVA – d, f, g, h].

773 **Figure 3. STIM1 deficiency causes enhanced type I IFN response in patient cells. a,**
774 Representative immunoblot showing expression of STIM1 in WT, *Stim1*^{-/-} MEFs or those expressing
775 either WT STIM1 (+STIM1) or STIM1^{E136X} (+E136X) mutant. **b,** qPCR analysis of *Irfn1* and *Ii6* mRNA
776 in indicated MEFs under resting conditions or 2 h after stimulation with 2',3'-cGAMP. Data show
777 representative triplicate from two independent experiments. **c,** Representative immunoblot showing
778 expression of STIM1 and GAPDH in PBMCs isolated from a healthy control (HC) and patient (Pat.). **d,**
779 Levels of indicated cytokines in serum samples from healthy controls (three independent donors) and
780 STIM1-deficient patient. Data show one representative triplicate from two independent experiments
781 (n=9 for three HCs). **e,** Taqman qPCR analysis of indicated ISGs from peripheral blood mononuclear
782 cells (PBMCs, top) or purified monocytes (below) from two independent healthy controls and STIM1-
783 deficient patient. Patient data (normalized to those of healthy controls) are derived from two
784 independent experiments performed in duplicates. Data are shown as mean ± s.e.m. *p < 0.05, **p <
785 0.005, ***p < 0.0005 (One-way ANOVA – b; and unpaired/two-tailed *t* test – d, e).

786

787 **Figure 4. STIM1 interacts with STING for its retention in the endoplasmic reticulum. a,**
788 Representative confocal microscopy image of STING-GFP and STIM1 in a MEF cell. Scale bar, 5 μm,
789 Inset – 1 μm. Pearson's *r* = 0.67 ± 0.08 from 9 cells. **b,** FLAG-immunoprecipitates (IP) from lysates of
790 HEK293T cells overexpressing FLAG-tagged STING and His-tagged STIM1 were immunoblotted for
791 detection of STIM1. Arrow, monomeric STING or STIM1; *, STING multimers. **c,** Immunoprecipitates
792 of endogenous STING from HEK293 cells were immunoblotted for detection of indicated proteins. **d,**
793 FLAG-immunoprecipitates (IP) from lysates of HEK293T cells expressing FLAG-tagged STING and
794 His-tagged STIM1 with or without treatment with thapsigargin (1 μM, 10 min; left) or 2', 3'-cGAMP (1
795 μM, 30 min and further incubation in media for 1 h) were immunoblotted for detection of the indicated
796 proteins. Bar graphs show densitometry analysis of normalized fold changes (mean ± s.e.m.) in
797 STIM1 and STING band intensity from three (left) and four (right) independent experiments. **e,**
798 Schematic showing domain structure of STING and STIM1 as indicated in the text. Amino acid

799 residues of STING and STIM1 fragments used in this study are indicated. **f**, Left – FLAG-
800 immunoprecipitates (IP) from lysates of HEK293T cells expressing FLAG-tagged full-length STING
801 (FL), NTD (a.a. 1-140), and CTD (a.a. 140-379) were immunoblotted for detection of STIM1. Right –
802 Purified recombinant GST-fused indicated fragments of STIM1 incubated with lysates of HEK293T
803 cells expressing FLAG-tagged, FL, NTD or CTD of STING were immunoblotted with anti-FLAG
804 antibody. Immunoblots in panels **b**, **c**, and **f** are representative of four independent experiments. * $p <$
805 0.005 (unpaired/two-tailed t test - d).

806

807 **Figure 5. STIM1 inhibits STING trafficking to the ER-Golgi intermediate compartment. a,**
808 Representative confocal microscopy images of WT or *Stim1*^{-/-} MEFs stably expressing STING-GFP
809 under resting conditions (top two panels) or 4 h after HSV-1 infection (bottom 3 panels) and stained
810 for endogenous p58 (ERGIC). Scale bars, 10 μ m. Bar graph shows quantification of indicated number
811 of cells showing STING translocation to the ERGIC under resting conditions or after infection with
812 HSV-1 for indicated times. Data are derived from two independent experiments. **b**, Representative live
813 cell epifluorescence images of WT (top) or *Stim1*^{-/-} (bottom) MEFs after treatment with 1 μ M 2', 3'-
814 cGAMP for the indicated times showing translocation of STING-GFP into the ERGIC (left). Line graph
815 on the right shows normalized rate of translocation of STING in WT (9 cells) and *Stim1*^{-/-} (11 cells)
816 MEFs from two independent experiments. Scale bar, 10 μ m. **c**, Reporter assays for *Irfb1* promoter
817 activity in HEK293T cells transfected with STING and increasing amounts of full length STIM1 or its
818 indicated fragments, 6 hours after stimulation with 2', 3' cGAMP (top) or poly(I:C) (below). Data show
819 representative triplicate from two independent experiments. * $p <$ 0.005, ** $p <$ 0.0005 Chi square test
820 (a) and one-way ANOVA (c); N.S. – not significant.

821

822 **Figure 6. Ablation of STIM1 enhances host defense towards DNA viruses and HIV by priming**
823 **type I IFN responses. a**, qPCR analysis of *Irfb1* and GFP transcripts in uninfected or HSV-1-GFP-
824 infected (MOI 0.1, 24 h) WT or *Stim1*^{-/-} MEFs. Data show pooled technical replicates from two

825 independent experiments. **b**, qPCR analysis of GFP and indicated viral mRNAs in MHV-68-GFP-
826 infected (MOI 0.2, 24 h) WT or *Stim1*^{-/-} MEFs. Data show pooled technical replicates from three
827 independent experiments. **c**, Representative immunoblots showing expression of phospho-IRF3 (P-
828 IRF3), total IRF3, and β -actin from untreated or HSV-1-infected (MOI 5.0) WT or *Stim1*^{-/-} MEFs for
829 indicated time points. **d**, qPCR analysis of *Ifnb1* and *Il6* mRNA in untreated or HSV-1-GFP-infected
830 (indicated MOI, 24 h) WT or *Stim1*^{-/-} BMDMs. Data shows representative triplicate from two
831 independent experiments. **e**, Top two panels show representative GFP images in HSV-1-GFP-
832 infected (MOI 10, 24 h) WT, (left) and *STIM1*^{-/-} (right) THP-1 cells. Below: qPCR analysis of *IFNB1*
833 and GFP transcripts from the same cells. Scale bars, 10 μ m. Data shows representative triplicate from
834 two independent experiments. **f**, Representative flow plots showing frequency of HIV-GFP-infected
835 WT (left) or two different *STIM1*^{-/-} (right two panels) THP1 cell lines (MOI 2.0, 24 h). Bar graph shows
836 averaged frequency of HIV-GFP-positive indicated THP1 cell lines in the presence or absence of HIV
837 reverse transcriptase inhibitor azidothymidine (AZT, 5 μ M) from four independent experiments.
838 Immunoblots in panel **c** and epifluorescence images in panel **e** are representative of three and two
839 independent experiments respectively. *p < 0.005 and **p < 0.0005 [Two-way ANOVA – a (left panel),
840 d, e (right panel), f; unpaired/two-tailed *t* test – a (right panel), b; One-way ANOVA – e (left panel)].

841

842 **Figure 7. STIM1 deficiency enhances host defense against HSV-1 infection in vivo.** **a**, Kinetics of
843 survival (top) and body weight changes (bottom) of indicated numbers of control (*Stim1*^{fl/fl}) and STIM1-
844 deficient (*Stim1*^{fl/fl}*Lyz2-cre*) mice (6-7-week old) after intravenous injection with HSV-1 (1 x 10⁷ PFU
845 per mouse). **b**, Kinetics of survival (top) and body weight changes (bottom) of indicated numbers of
846 control (*Orai1*^{fl/fl}) and Orai1-deficient (*Orai1*^{fl/fl}*Lyz2-cre*) mice after intravenous injection with HSV-1 (1
847 x 10⁷ PFU per mouse). Mice that lost >20% body weight were euthanized. **c**, Virus load in control
848 (*Stim1*^{fl/fl}) and STIM1-deficient (*Stim1*^{fl/fl}*Lyz2-cre*) mouse brains 3 days after intravenous injection with
849 HSV-1. **d**, ELISA analyses of the indicated cytokines from the sera of control (*Stim1*^{fl/fl}) and *Stim1*-
850 deficient (*Stim1*^{fl/fl}*Lyz2-cre*) mice after intravenous injection with HSV-1 for indicated times. Data in

851 panels **a** and **b** are pooled from two independent experiments. Panels **c** and **d** show mean +/- s.e.m.
852 from indicated number of animals (each symbol represents data from individual animal). *p < 0.05, **p
853 < 0.005, ***p < 0.0005 (unpaired/two-tailed *t* test).

854

855

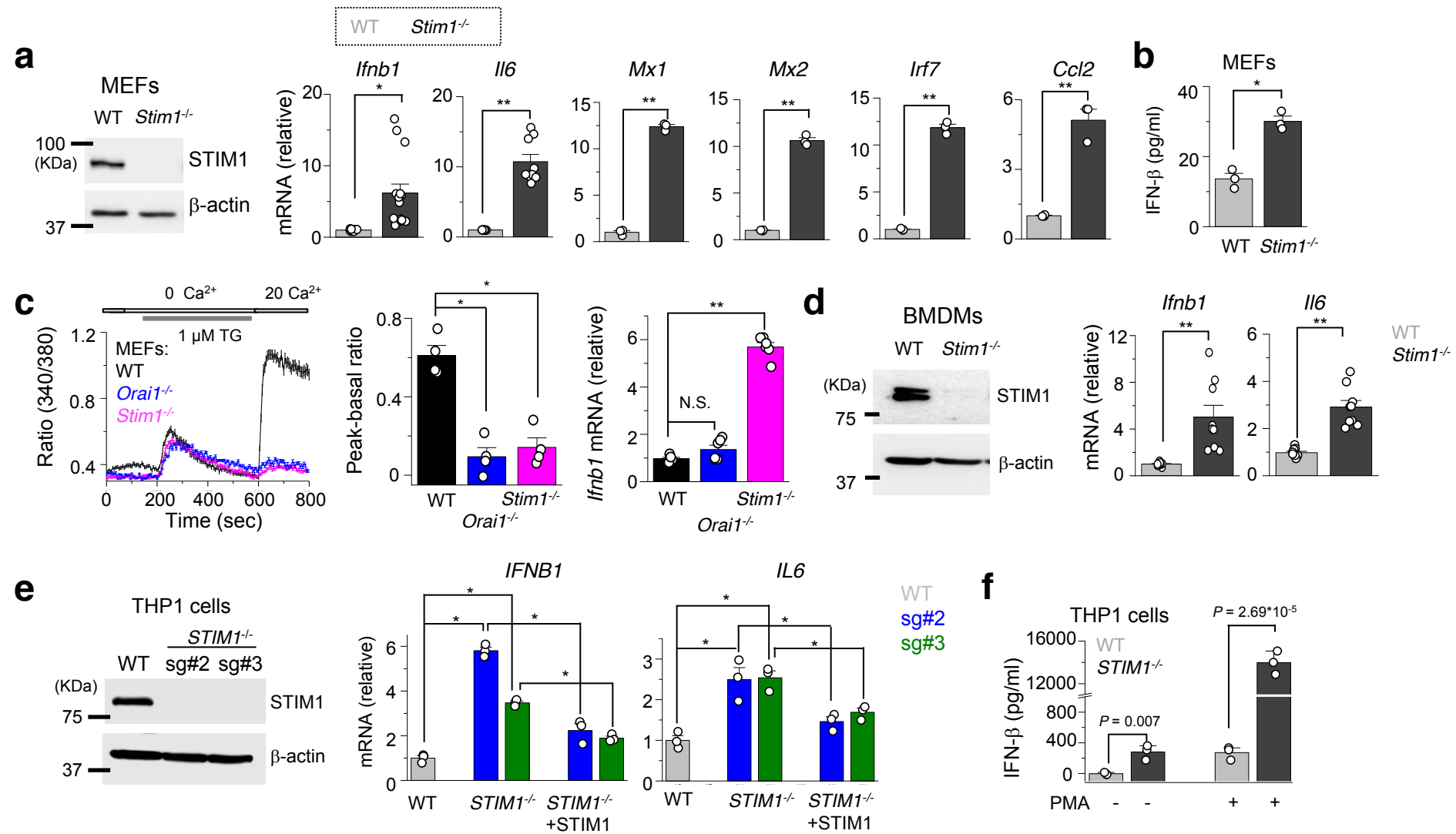


Figure 1

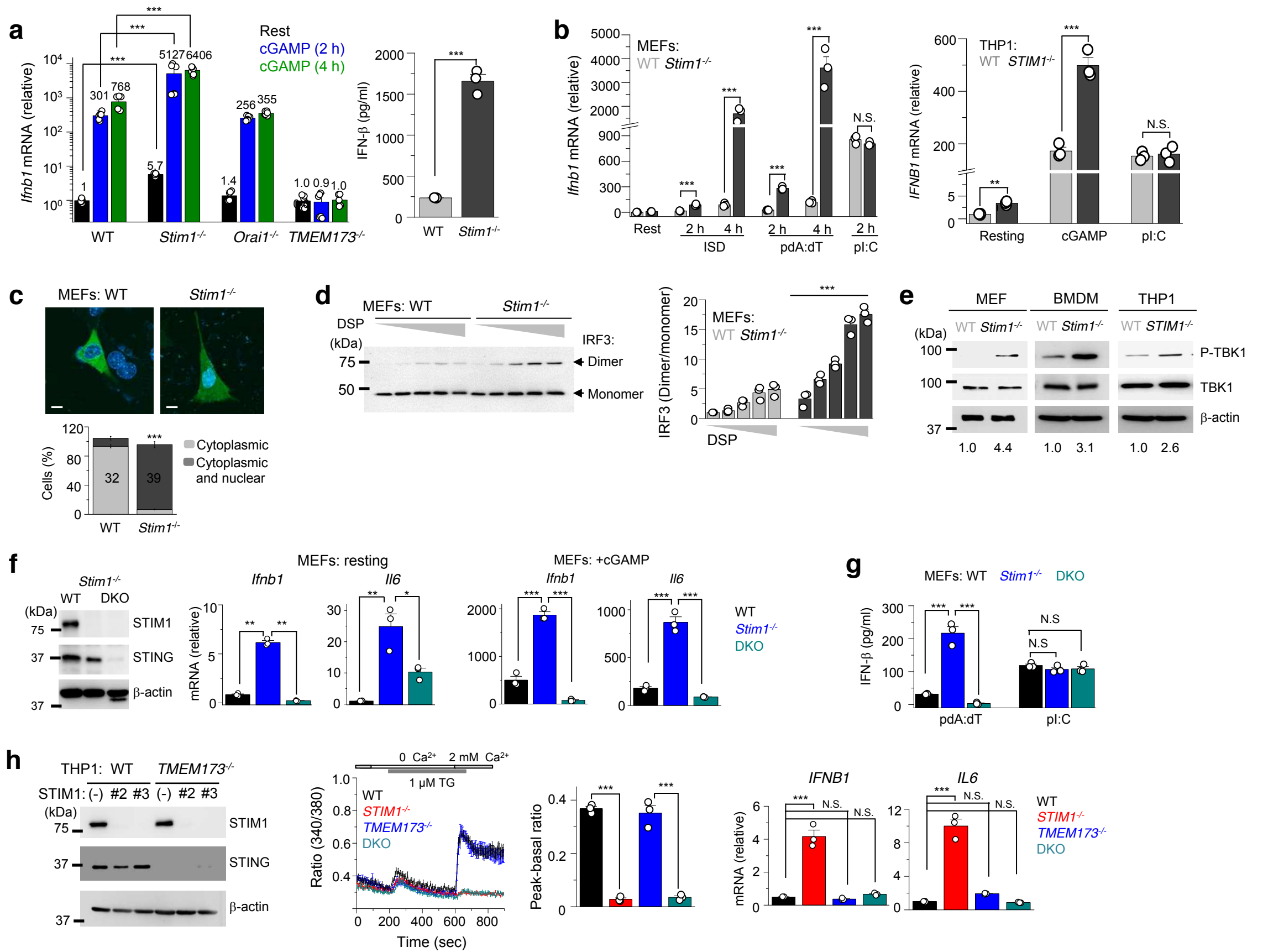


Figure 2

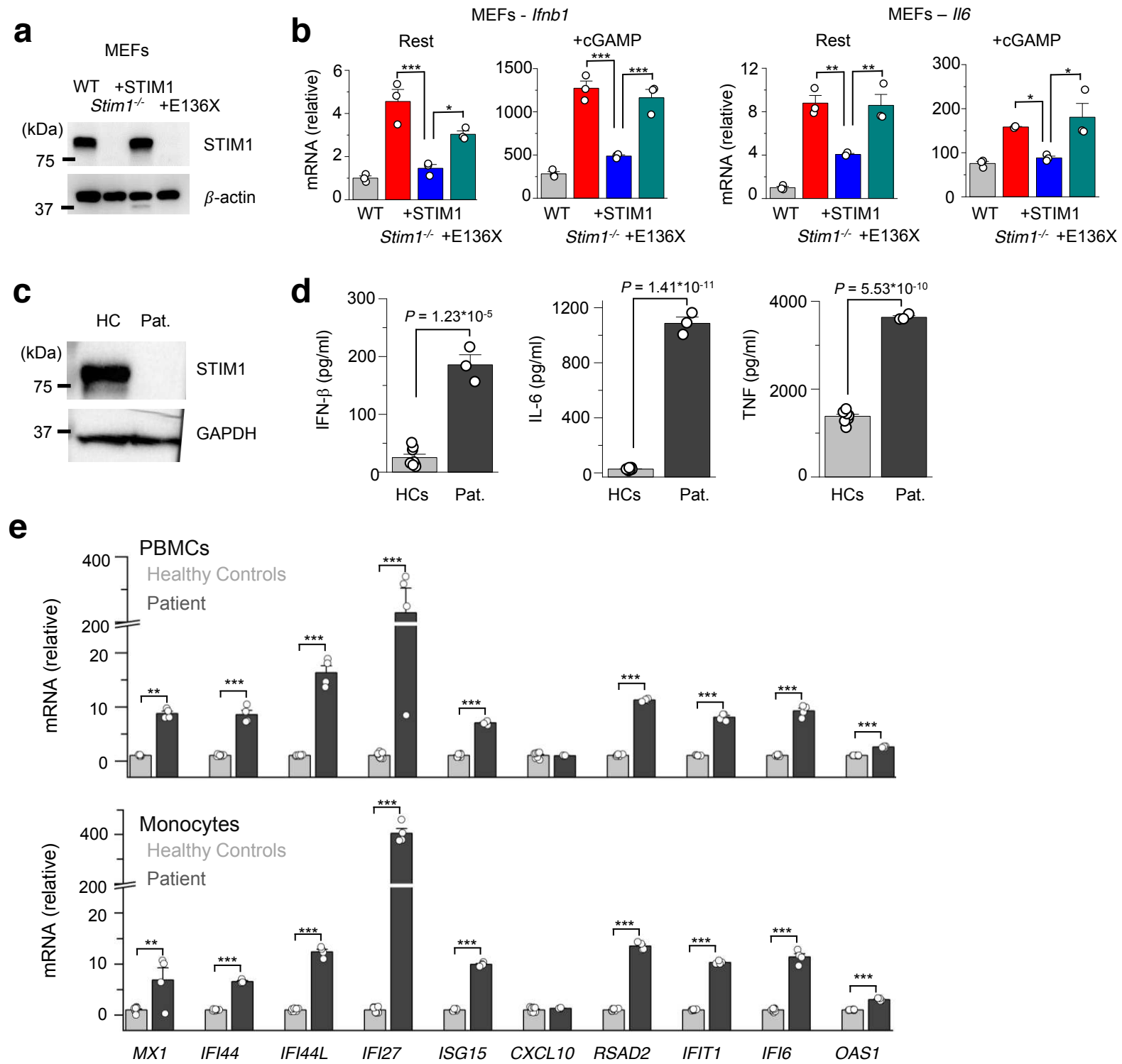


Figure 3

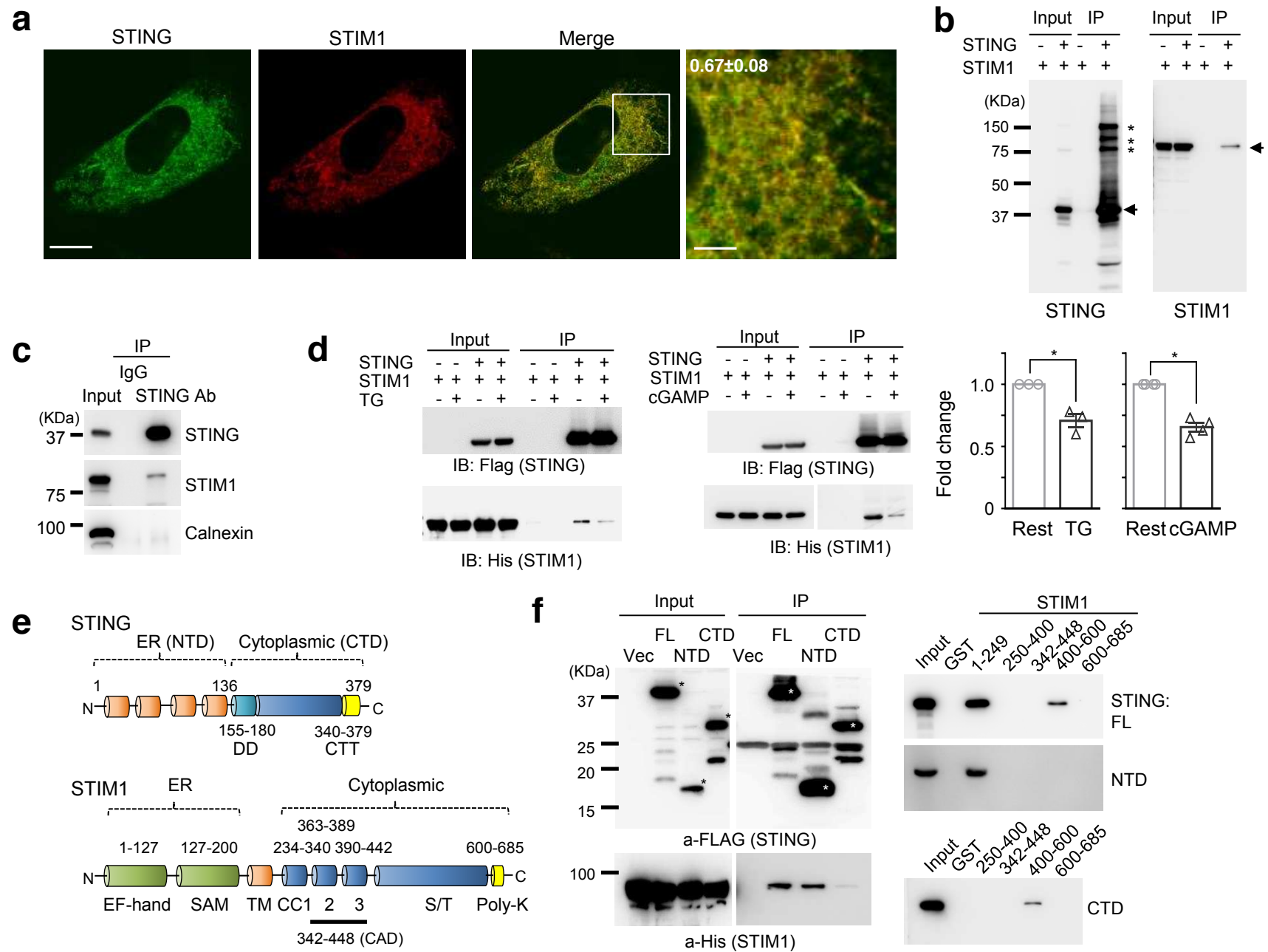


Figure 4

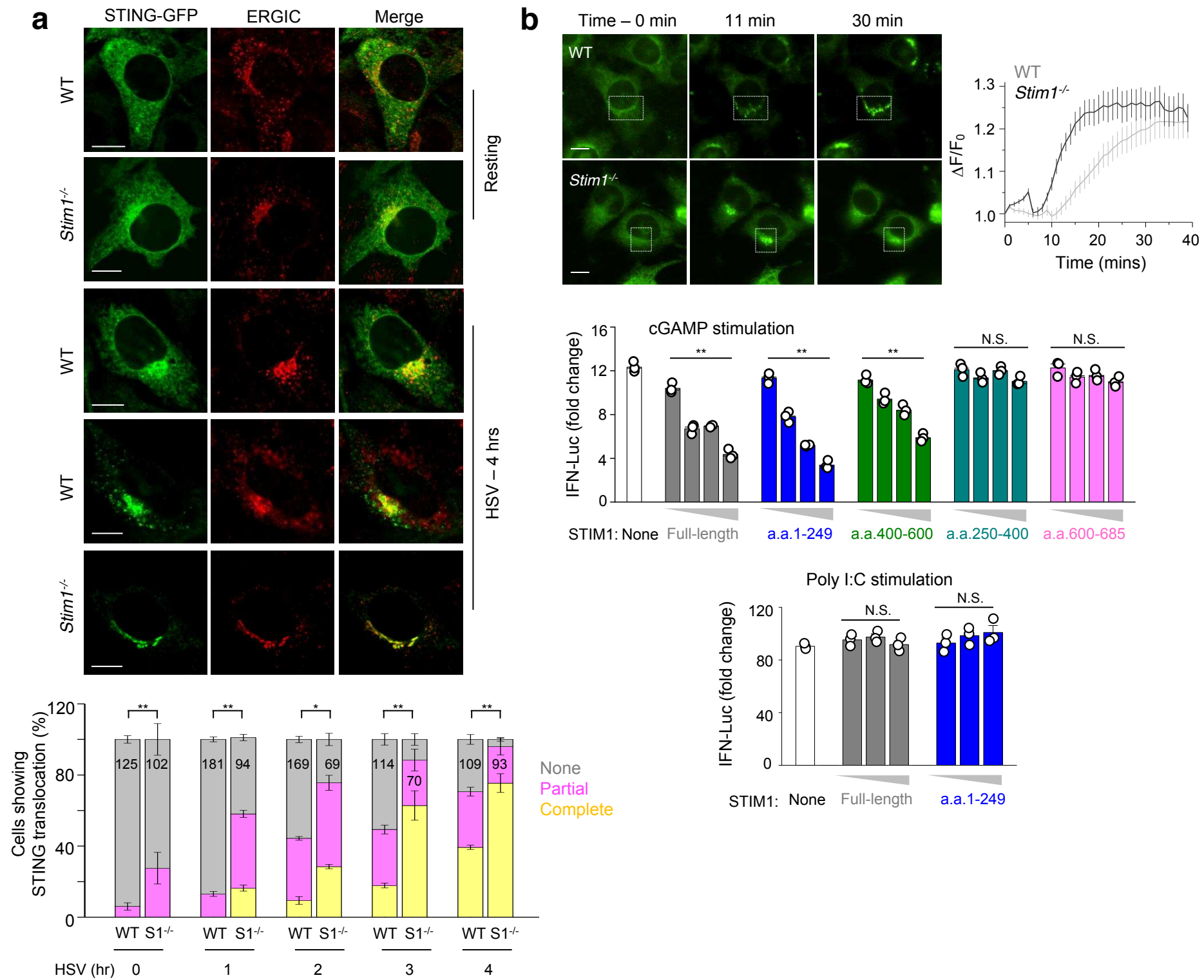


Figure 5

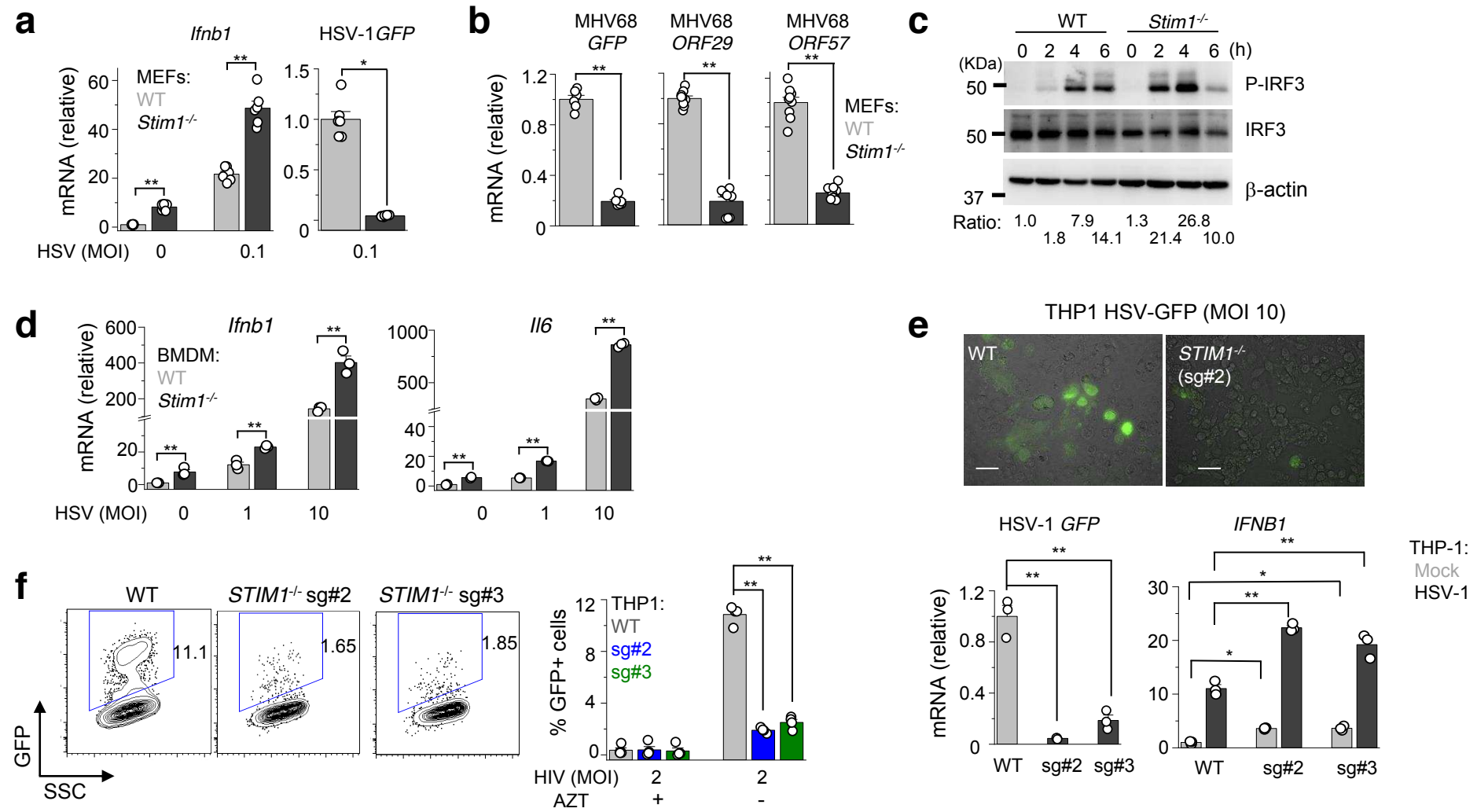


Figure 6

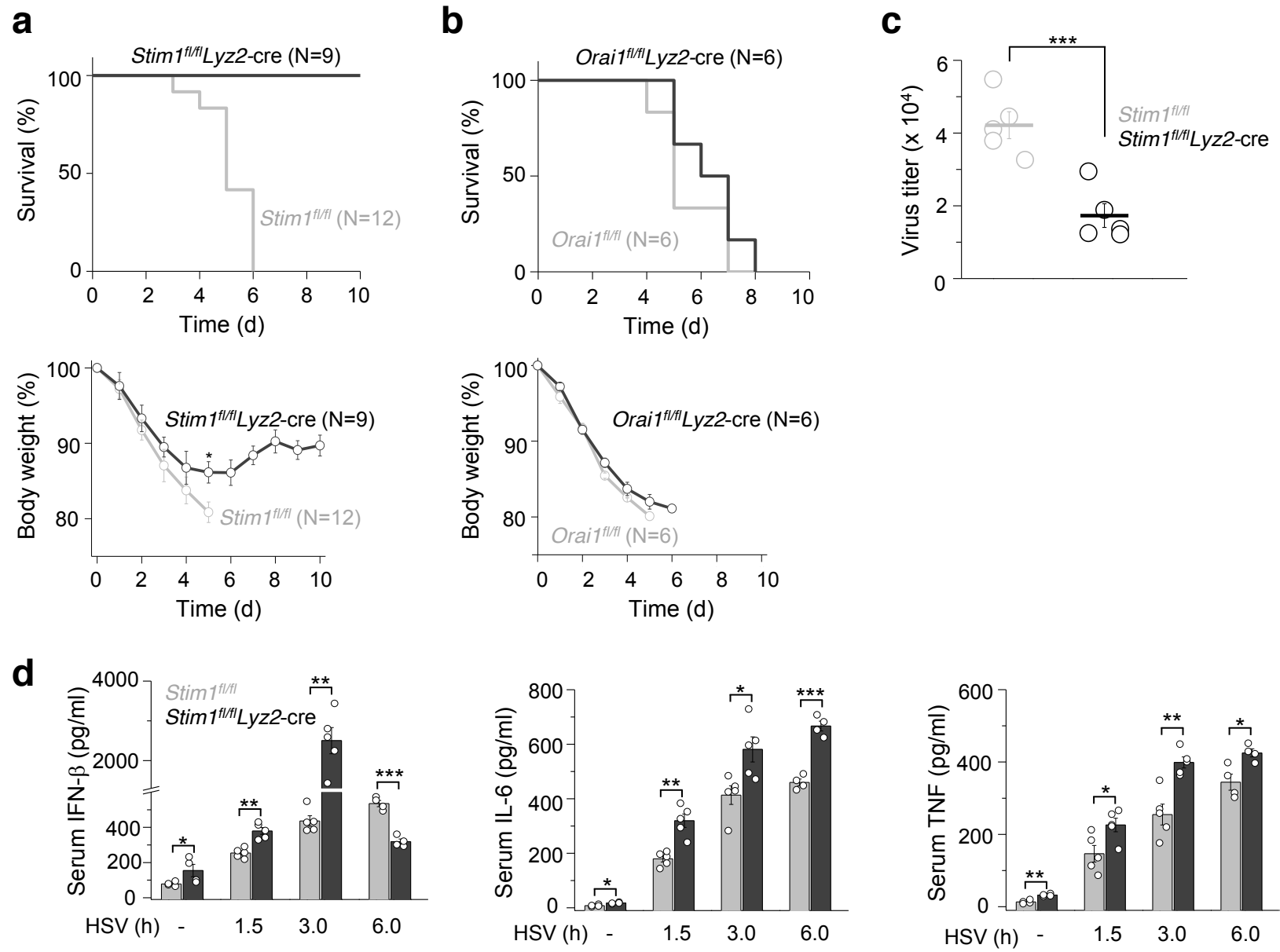
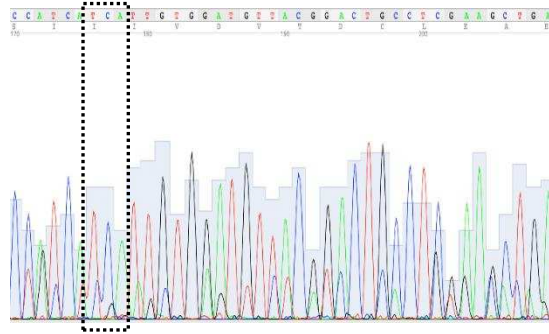


Figure 7

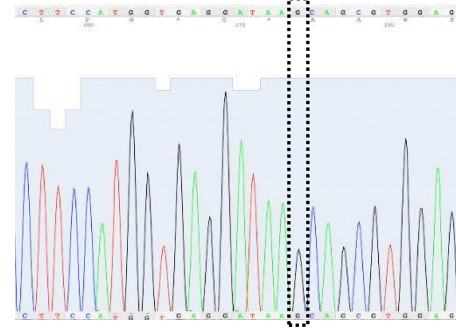
Exon 2

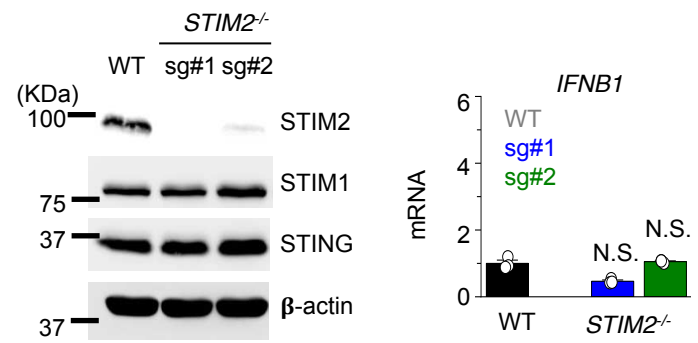
hSTIM1 CCATCAG-^{*}TTTGTGGATGTTACGGACTGCCTCGAAGCTGA
sg#2 CCATCATCATTTGTGGATGTTACGGACTGCCTCGAAGCTGA

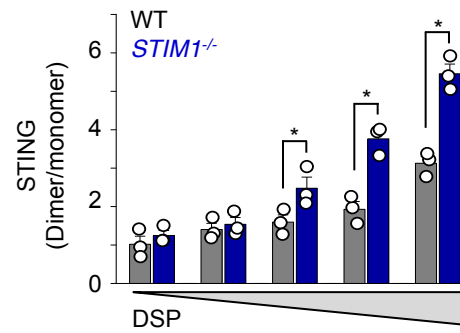
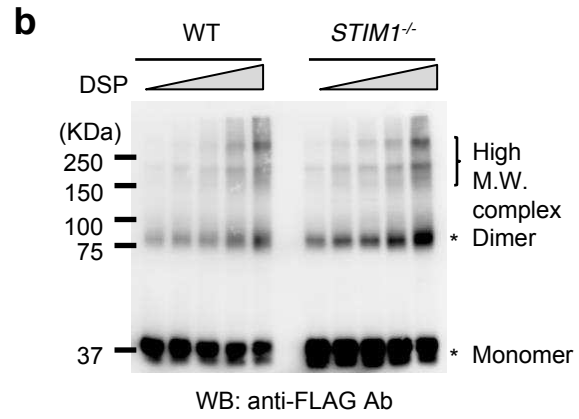
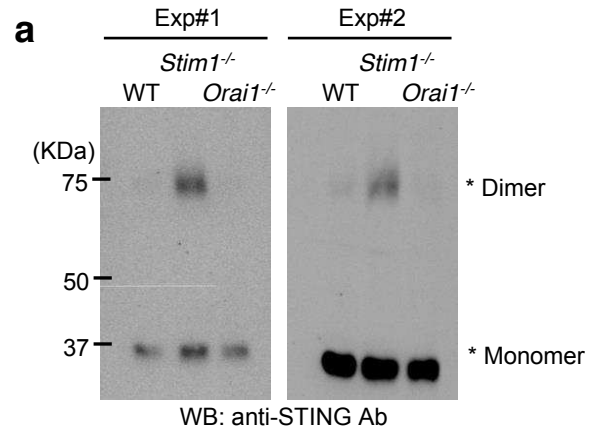


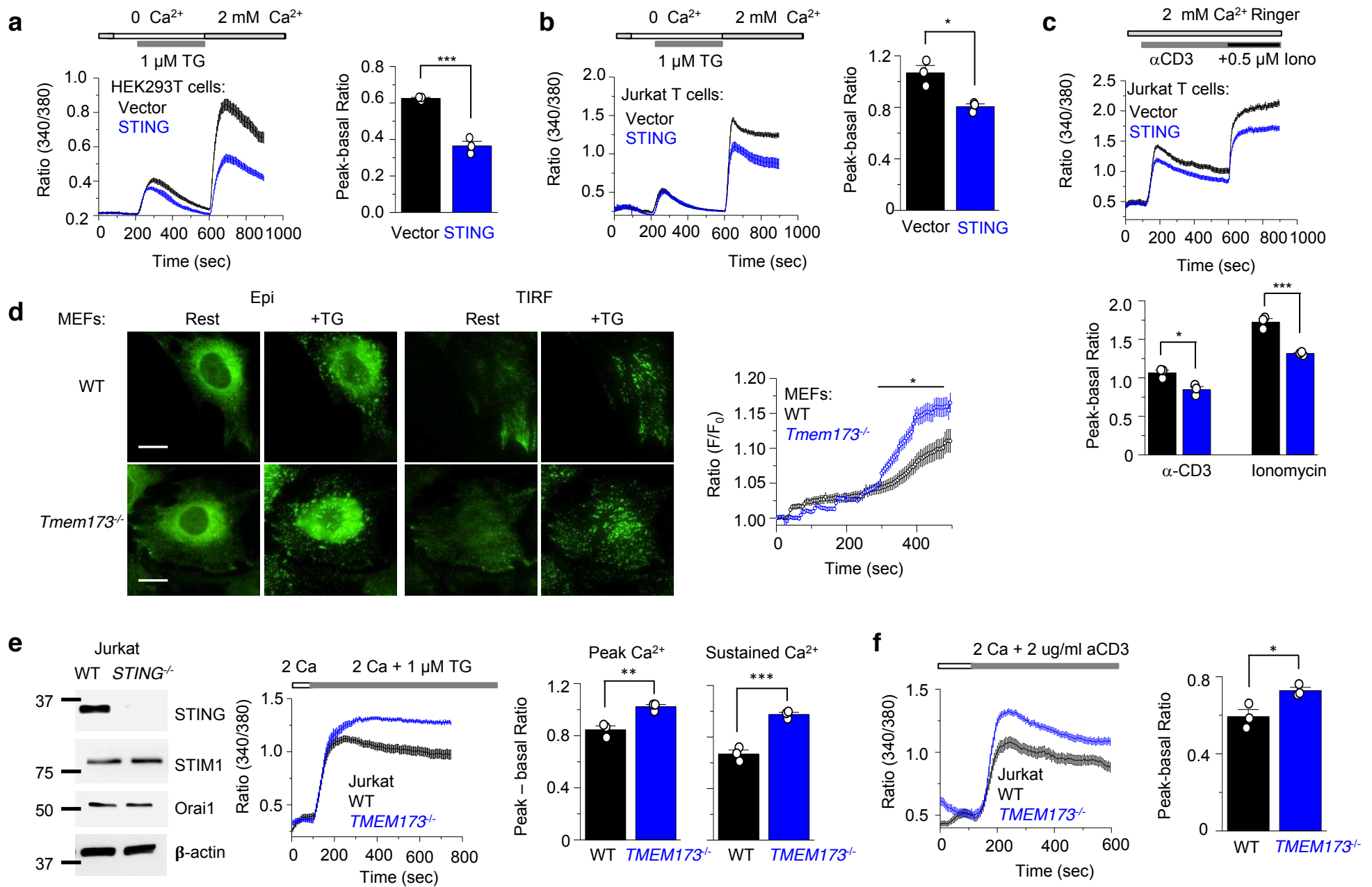
Exon 3

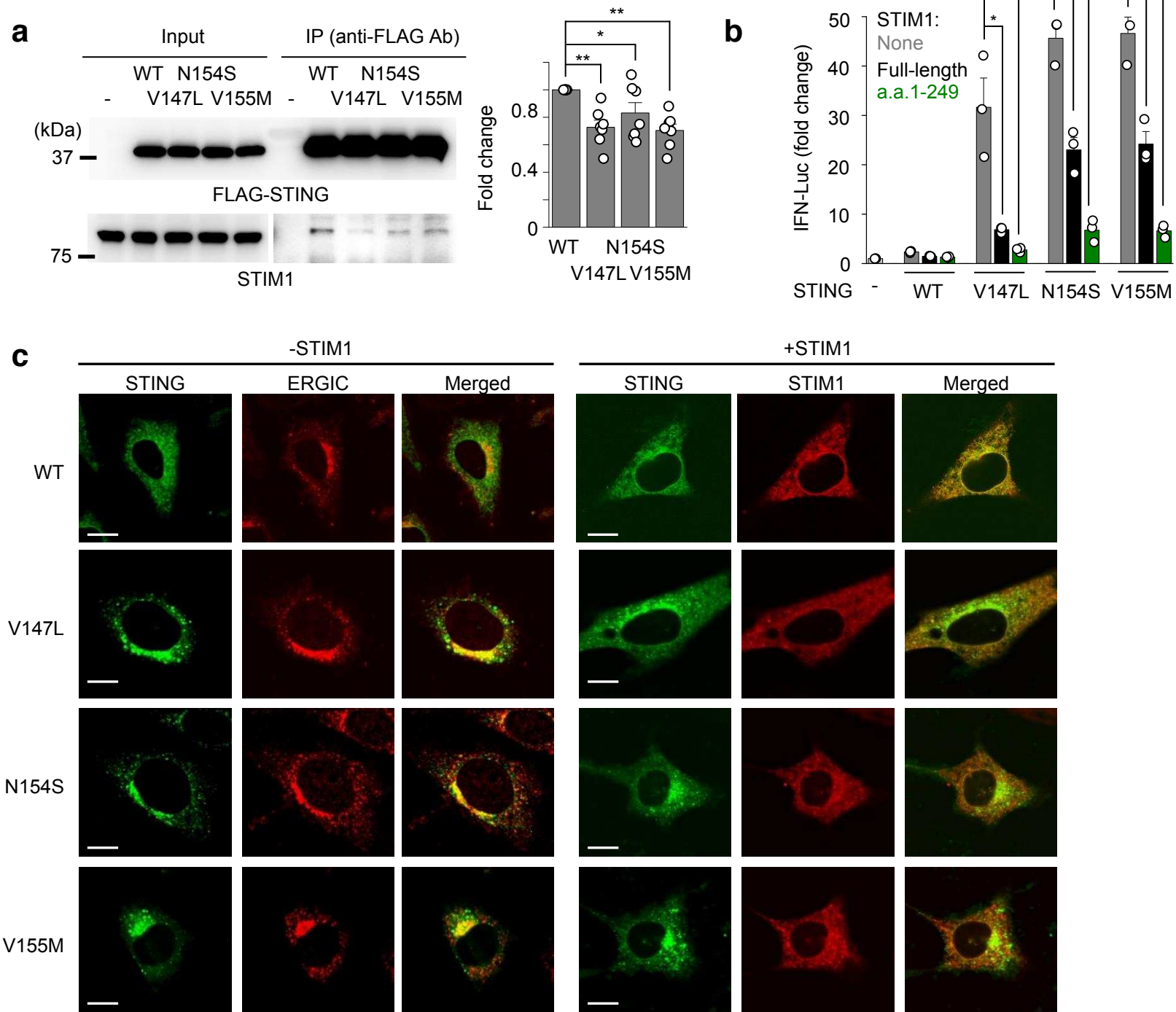
hSTIM1 CTTCCATGGTGAGGATAAGCTCATCAGCGTGGAGG.
sg#3 CTTCCATGGTGAGGATAA----GCAGCGTGGAGG.

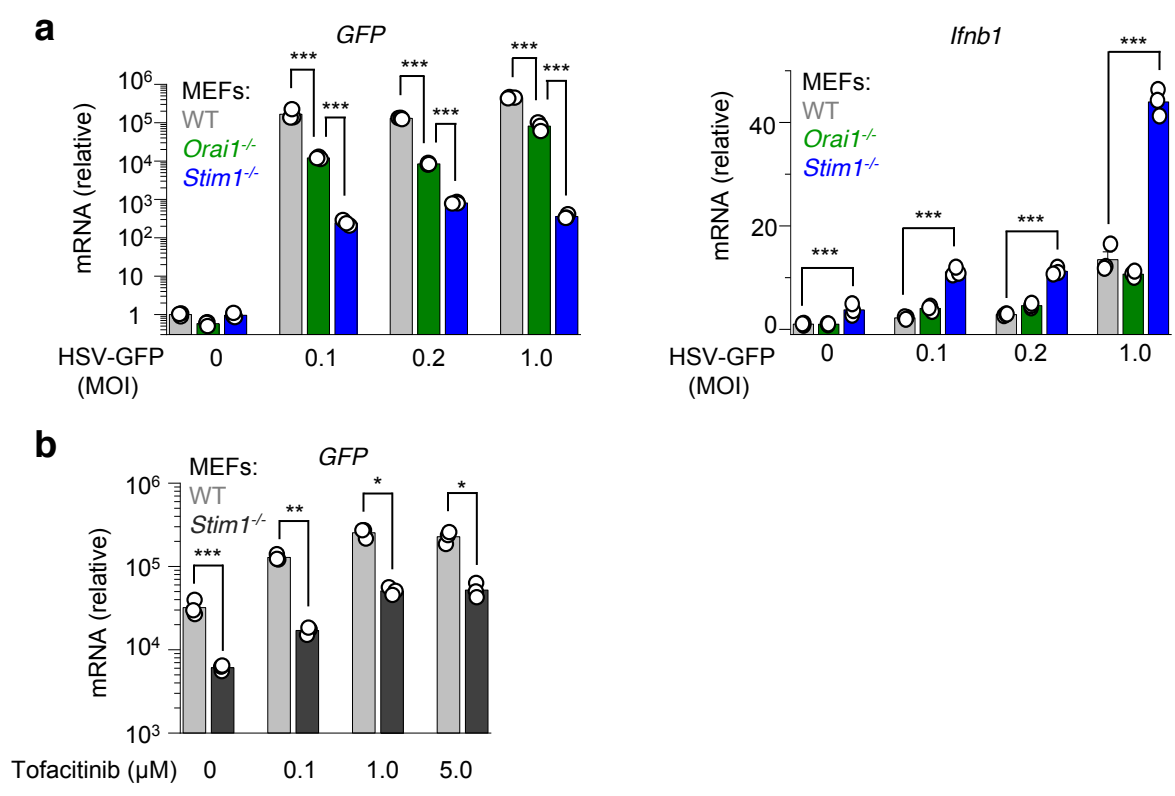


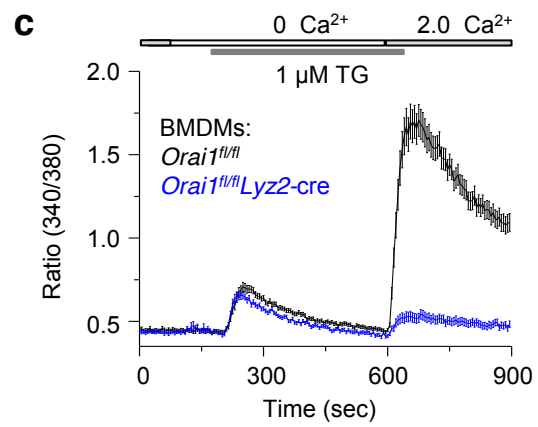
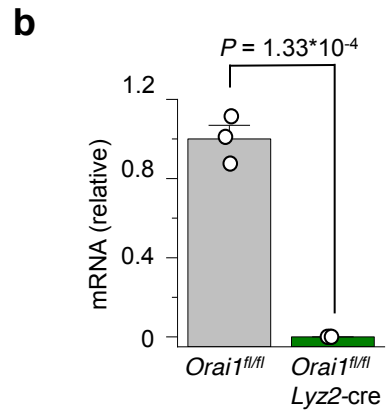
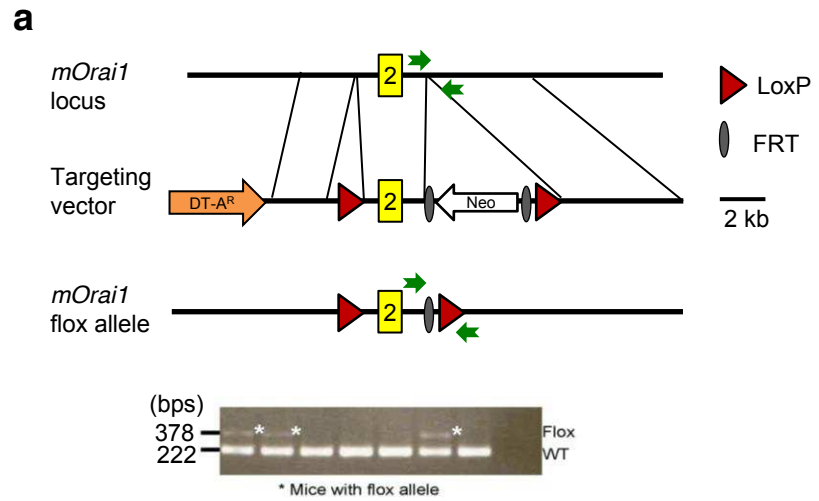












1 **SUPPLEMENTAL INFORMATION**

2 **Supplementary Table**

3 **Supplementary Table 1. List of primers and sgRNAs used in this study**

4

Gene name	Forward Primer	Reverse Primer	Comments
<i>STIM1</i> _pLentiguide_sg1	CACCGCATCATCGTCCATCAGT TTG	AAACCAAAGTATGGACGATGAT GC	sgRNA targeting human STIM1
<i>STIM1</i> _pLentiguide_sg2	CACCGCCGTAACATCCACAAA CTGA	AAACTCAGTTTGTGGATGTTACG GC	sgRNA targeting human STIM1
<i>STIM1</i> _pLentiguide_sg3	CACCGTGAGGATAAGCTCATC AGCG	AAACCGCTGATGAGCTTATCCTC AC	sgRNA targeting human STIM1
<i>STIM2</i> _pLentiguide_sg1	CACCGAGAAGAAGACAGATTTA GTC	AAACGACTAAATCTGTCTTCTTCT C	sgRNA targeting human STIM2
<i>STIM2</i> _pLentiguide_sg2	CACCGAGATGGTGAATTGAA GTAG	AAACCTACTTCAATTCCACCATCT C	sgRNA targeting human STIM2
<i>STIM2</i> _pLentiguide_sg3	CACCGAGATAAACATATAACGA TTG	AAACCAATCGTTATATGTTTATCT C	sgRNA targeting human STIM2
<i>TMEM173</i> _pLentiguide_sg	CACCGAATATGACCATGCCAG CCCA	AAACTGGGCTGGCATGGTCATAT TC	sgRNA targeting human STING
<i>Ifnb</i>	AACCTCACCTACAGGGCGGAC TTCA	TCCCACGTCAATCTTTCCTCTTGC TTT	sgRNA targeting human STIM1

<i>Mx1</i>	GACCATAGGGGTCTTGACCAA	AGACTTGCTCTTTCTGAAAAGCC	qPCR primers
<i>Mx2</i>	GAGGCTCTTCAGAATGAGCAA A	CTCTGCGGTCAGTCTCTCT	qPCR primers
<i>Irf7</i>	GAGACTGGCTATTGGGGGAG	GACCGAAATGCTTCCAGGG	qPCR primers
<i>Ccl2</i>	TTAAAAACCTGGATCGGAACCA A	GCATTAGCTTCAGATTTACGGGT	qPCR primers
<i>Ii6</i>	ACAACCACGGCCTTCCCTACTT	CACGATTTCCCAGAGAACATGT	qPCR primers
<i>36b4</i>	AGATTCGGGATATGCTGTTGG C	TCGGGTCCTAGACCAGTGTTTC	qPCR primers
<i>IFNB</i>	AGGACAGGATGAACTTTGAC	TGATAGACATTAGCCAGGAG	qPCR primers
<i>IL6</i>	CCAGCTATGAACTCCTTCTC	GCTTGTTCTCACATCTCTC	qPCR primers
<i>36B4</i>	AGATGCAGCAGATCCGCAT	GTTCTTGCCCATCAGCACC	qPCR primers
<i>MO70_TM173</i>	GCG CTC GAG ATG CCC CAC TCC AGC CTG	GCG GAA TTC AGA GAA ATC CGT GCG GAG	Sub-cloned in MO70 using XhoI and EcoRI sites
<i>MO70_TM173_TM</i>	CCG CTC GAG ATG CCC CAC TCC AGC CTG	CGG AAT TCG TTG AAA TTC CCT TTT TC	Sub-cloned in MO70 using XhoI and EcoRI sites
<i>MO70_TM173_CTD</i>	CCG CTC GAG ATG GAA AAA GGG AAT TTC AAC	CGG AAT TCA GAG AAA TCC GTG CGG AG	Sub-cloned in MO70 using XhoI and EcoRI sites
<i>MO70_TM173_V147L</i>	GAG ATC TCT GCA TTG TGT GAA AAA G	CTT TTT CAC ACA ATG CAG AGA TCT C	Site directed

			mutagenesis
MO70_ <i>TMEM173</i> _N154S	AAG GGA ATT TCA GCG TGG CCC ATG G	CCA TGG GCC ACG CTG AAA TTC CCT T	Site directed mutagenesis
MO70_ <i>TMEM173</i> _V155M	GGG AAT TTC AAC ATG GCC CAT GGG C	GCC CAT GGG CCA TGT TGA AAT TCC C	Site directed mutagenesis
GFP	AAGCTGACCCTGAAGTTCATCT GC	CTTGTAGTTGCCGTCGTCCTTGA A	qPCR primers
<i>MHV68_ORF29</i>	CCA CCA AAA ACA TGT GTC CT	TTG CTG GAA GTG CTT CCT TCT	qPCR primers
<i>MHV68_ORF57</i>	GACCAAATGATGGAAGGAC	GCAGAGGAGAGTTGTGGAC	qPCR primers
pEGFPC1_ <i>Tmem173</i>	AGA TCT CGA GCT ATG CCA TAC TCC AAC CTG CAT	GCG GAA TTC TCA GAT GAG GTC AGT GCG GAG	Murine STING in pEGFPC1 vector using XhoI and EcoRI sites
Interferon Stimulatory DNA (ISD)	TACAGATCTACTAGTGATCTAT GACTGATCTGTACATGATCTAC A	TGTAGATCATGTACAGATCAGTC ATAGATCACTAGTAGATCTGTA	
<i>Orai1</i> _Flox_Genotyping	AGGCGGCCTATAATTCCAGCTT CA	AGGTGGATGTTGCTGAGAGACCA A	WT band 222 bps, Flox band – 378 bps
<i>Orai1</i> _cKO_Genotyping	GATTGACAGTGGCAGTGTTC CAA	TCCTGTTTAAGCTAACAAGGAGC GGC	220 bps KO band

5

6

7

8 **Supplementary Figure Legends:**

9 **Supplementary Figure 1. Sequencing data for *STIM1*^{-/-} THP1 clones generated using CRISPR-**
10 **Cas9 system.** Top - alignment of sequences within exon 2 and 3 of human *STIM1* gene with the ones
11 from individual clones (sg# 2 and sg#3). The sgRNA sequences are highlighted in red. Below –
12 Sequencing results of individual clones. Boxed areas mark the indel sites. Clone sg#2 shows insertion
13 of 3 nucleotides and deletion of 2 nucleotides whereas sg#3 shows deletion of 5 nucleotides.

14 **Supplementary Figure 2. Lack of spontaneous induction of the type I IFN response in *STIM2*^{-/-}**
15 **THP1 cells.** Left – Immunoblot showing expression of STIM2 in control or *STIM2*^{-/-} THP1 cells
16 generated using two independent sgRNAs (sg#1 and sg#2). Loss of STIM2 does not alter expression
17 of STIM1 or STING in these cells. Right - qPCR analysis of *IFNB1* transcripts in unstimulated control
18 and *STIM2*^{-/-} THP1 cells. N.S. – not significant. Data shows representative triplicate from two
19 independent experiments.

20 **Supplementary Figure 3. STIM1 deficiency induces dimerization of STING.** **a**, Immunoblots from
21 two representative experiments (Exp #1 and #2) showing endogenous STING in control, *Stim1*^{-/-} and
22 *Orai1*^{-/-} MEFs under non-reducing SDS PAGE conditions. * indicates the position of monomeric and
23 dimeric STING. **b**, Lysates from untreated or DSP-treated (0.125, 0.25, 0.5, 1.0 and 2.0 mM, 1 hour
24 on ice) control or *STIM1*^{-/-} HEK293T cells expressing STING-FLAG were immunoblotted for detection
25 of STING under non-reducing conditions (left). Bar graph shows averaged ratio of STING
26 (dimer/monomer) from three independent experiments (right). *p < 0.05 (unpaired/two-tailed *t* test).

27 **Supplementary Figure 4. Overexpression or deletion of STING affects SOCE and STIM1**
28 **translocation kinetics.** **a**, Representative traces of averaged SOCE from HEK293T cells expressing
29 empty vector (24 cells) or that encoding STING (27 cells) after passive depletion of intracellular Ca²⁺
30 stores with 1 μM thapsigargin in the presence of external solution containing 2 mM Ca²⁺ as indicated.
31 **b**, Representative traces of averaged SOCE from Jurkat T cells expressing empty vector (54 cells) or
32 that encoding STING (49 cells). **c**, Representative traces of averaged SOCE from Jurkat T cells
33 expressing empty vector (49 cells) or that encoding STING (53 cells) after stimulation with 10 μg/ml of
34 α-CD3 antibody or 0.5 μM ionomycin in the presence of external solution containing 2 mM Ca²⁺ as
35 indicated. **d**, Representative epifluorescence (left) and total internal reflection fluorescence (TIRF,
36 right) images of WT or *Sting*^{-/-} MEFs stably expressing STIM1-YFP under resting conditions or 10
37 mins after depletion of intracellular Ca²⁺ stores using 1 μM thapsigargin (TG). Scale bar, 10 μm. Line
38 graph on the right shows mean normalized fluorescence intensity ± s.e.m. of STIM1-YFP in WT (6
39 cells) and *Tmem173*^{-/-} MEFs (9 cells) from two independent experiments. **e**, Left – Immunoblot
40 showing expression of indicated proteins in control and *TMEM173*^{-/-} Jurkat T cells. Right panels show
41 representative traces of averaged SOCE from control (54 cells) and *TMEM173*^{-/-} (58 cells) Jurkat T

42 cells. **f**, Representative traces of averaged SOCE from control (66 cells) and *TMEM173*^{-/-} (60 cells)
43 Jurkat T cells after stimulation with anti-CD3 antibody (2 g/ml) in the presence of external solution
44 containing 2 mM Ca²⁺ as indicated. Bar graphs in panels **a-c**, **e** and **f** show averaged baseline
45 subtracted peak SOCE (\pm s.e.m.) from three independent experiments. *p<0.05, **p < 0.005,
46 ***p<0.0005 (unpaired/two-tailed *t* test).

47 **Supplementary Figure 5. Functional Interaction of constitutively active STING mutants with**
48 **STIM1.** **a**, FLAG-immunoprecipitates (IP) from lysates of HEK293T cells stably expressing FLAG-
49 tagged WT or indicated mutants of STING were immunoblotted for detection of endogenous STIM1
50 proteins (left). Bar graph (right) shows densitometry analysis of normalized (relative to WT STING)
51 fold change in STIM1 band intensity from seven independent experiments. **b**, Reporter assay for *Irf3*
52 promoter activity in HEK293T cells transfected with WT or mutant STING proteins and full-length
53 STIM1 or its N-terminal fragment (a.a. 1-249) for 24 hours (right). Data shows representative triplicate
54 from two independent experiments. **c**, Representative confocal microscopy images of MEFs stably
55 expressing WT STING-GFP or indicated SAVI mutants without or with STIM1. Cells were either
56 stained for endogenous p58 (ERGIC marker, left three panels) or STIM1 (+ STIM1, right three
57 panels). Scale bar, 10 μ m. Images are representative of 25-30 cells for each condition. *p < 0.05, **p
58 < 0.005, and ***p < 0.0005 (unpaired/two-tailed *t* test – a; One-way ANOVA - b).

59 **Supplementary Figure 6. STIM1 plays a Ca²⁺-independent role in the anti-viral immune**
60 **response.** **a**, qPCR analysis of GFP (left) and *Irf3* (right) transcripts in WT, *Orai1*^{-/-} or *Stim1*^{-/-} MEFs
61 uninfected or HSV-1-GFP-infected with indicated MOI. **b**, qPCR analysis of GFP (left) transcripts in
62 HSV-GFP-infected (MOI 0.5, 24 hours) WT or *Stim1*^{-/-} MEFs in the presence or absence of indicated
63 amounts of tofacitinib. Cells were preincubated with the inhibitor for 30 mins prior to infection. Data
64 shows representative triplicate from two independent experiments. Data are shown as mean \pm s.e.m.
65 *p < 0.05, **p < 0.005, and ***p < 0.0005 (Two-way ANOVA – a; unpaired/two-tailed *t* test -b).

66 **Supplementary Figure 7. Generation of conditionally targeted Orai1-deficient mice.** **a**,
67 Schematic showing the architecture of mouse *Orai1* gene. Exon 2 of the *Orai1* gene was targeted. By
68 homologous recombination, *Orai1*^{fl/fl} mice with loxP sites (red arrowheads) flanking exon 2 were
69 generated. Germ-line transmission of flox alleles was validated by genotyping PCR (lower panel). The
70 location of the primer pair is indicated as green (5' and 3') arrows. A 378 bp-band is derived from the
71 flox allele while a 200-bp band denotes the WT allele. **b**, qPCR analysis of *Orai1* transcripts in control
72 (*Orai1*^{fl/fl}) or *Orai1*^{-/-} BMDMs 7 days after differentiation. Data shows representative triplicate (mean \pm
73 s.e.m., unpaired/two-tailed *t* test) from two independent experiments **c**, Representative traces of
74 averaged SOCE from *Orai1*^{fl/fl} (36 cells) and *Orai1*^{-/-} (41 cells) BMDMs 7 days after differentiation and
75 after passive depletion of intracellular Ca²⁺ stores with 1 M thapsigargin in the presence of external
76 solution containing 2 mM Ca²⁺ as indicated. Data are representative of three independent
77 experiments.